Visualizing mRNA Translation *in situ* in Single Cells

Thesis by

Kelly Burke

In Partial Fulfillment of the Requirements for

the degree of

Doctor of Philosophy in Chemistry

CALIFORNIA INSTITUTE OF TECHNOLOGY

Pasadena, California

2018

(Defended July 10, 2017)

Kelly Burke
ORCID: 0000-0002-3615-9828

ACKNOWLEDGEMENTS

First, thanks to my advisor, Prof. David Tirrell, for his infectious curiosity about science and genuine care for his students. I am especially grateful that Dave took a chance on me. As a third-year graduate student, I asked Dave if I could join his group and work on a project completely unrelated to the typical research in his lab. Without hesitation, Dave agreed. Dave's openness to new ideas and belief in his students bring out the best creativity in people and are qualities I strive for in my own work.

Thanks to the members of my thesis committee, Prof. Jack Beauchamp, Prof. Bil Clemons, and Prof. Niles Pierce, for their support and advice. I thank Jack for serving as my committee chair and being available whenever I needed advice, whether related to my research or my personal goals. I thank Bil for always asking the 'big picture' questions about my research and encouraging me to think deeply about not just what I was doing but why. I thank Niles for sharing his expertise in nucleic acid hybridization technologies and meticulously developing methods in his lab that enabled me to carry out my research ideas. I also thank Dr. Harry Choi for his dedicated work building and perfecting these methods in Niles' lab.

Thanks to the entire Tirrell group, both present and past, for fostering a supportive and fun working environment. It is rare to find a group of individuals who are so excited about the success of their peers and offer them help in any way possible.

Thanks to my scientific mentors in my undergraduate education at Emory University. These individuals inspired my love for science and desire to never stop learning. In particular, thanks to my science professors at Oxford College of Emory University: Ms. Brenda Harmon, Dr. Lloyd Parker, Dr. Reza Saadein, Dr. Nitya Jacobs, and Dr. Steve Baker. Oxford is where my journey into science started, and I am grateful to have had professors who love what they are doing and truly care about the students they teach. Thanks to Dr. Khalid Salaita, who was one of the most encouraging professors I had at Emory and served on my undergraduate thesis committee. Thanks to Dr. Brian Dyer, my undergraduate research advisor. Dr. Dyer treated me as an

independent researcher from day one. He challenged me to think critically about my work and take ownership of my project. He graciously allowed me to attend multiple conferences and helped me publish my first research publication. I could not have asked for a more supportive undergraduate advisor. Thanks in particular to Dr. Dzmitry Parul (Dima), who was a postdoc in Dr. Dyer's lab and my first research mentor. Dima had the challenge of teaching me how to work in an academic research lab for the first time. I had so many questions and made so many mistakes, but Dima always responded with absolute patience and kindness. Thanks also to my best friends Diana Chen, Katie Slabach, Kaitlin Smith, and Jake Weiner for making my time at Emory an enjoyable one and for their continued friendship today.

Finally, thanks to my family for their love and support throughout all my life. Thanks to my grandparents, Paul and Mary Ann Traina, who generously funded my undergraduate education, which helped me discover my love for science and led me to pursuing my PhD. My grandparents taught me the value of education and giving back my knowledge to others. Thanks to my parents Jean Holmes and David Burke for having absolute faith in my abilities and decisions and always supporting me 100%. Thanks to my brother John Burke for being my best friend from day one and always making me laugh when I need it. Thanks to Timur Zhiyentayev for making me unafraid to learn new things and take a risk in life.

ABSTRACT

Translation of mRNA is tightly regulated in cells to ensure that proteins are synthesized at the right time, in the right location, and at appropriate levels. Single-molecule fluorescence *in situ* hybridization (smFISH) is a simple and widely used method to measure mRNA transcription through determining the abundance and localization of mRNAs in single cells. A comparable single-molecule *in situ* method to measure mRNA translation would enable a more complete understanding of gene regulation. In this thesis, we describe the development and characterization of a fluorescence assay to detect ribosome interactions with mRNA (FLARIM). The method adapts smFISH to visualize and characterize translation of single molecules of mRNA in fixed cells. To visualize ribosome-mRNA interactions, we use pairs of oligonucleotide probes that bind separately to ribosomes (via ribosomal RNA) and to the mRNA of interest, and that produce strong fluorescence signals via the hybridization chain reaction (HCR) when the probes are in close proximity. FLARIM does not require genetic manipulation, is applicable to practically any endogenous mRNA transcript, and provides both spatial and temporal information.

We first characterize FLARIM in mouse fibroblast cells. We show that FLARIM is sensitive to changes in ribosome association with mRNA upon inhibition of global translation with puromycin. We also show that FLARIM detects changes in ribosome association with an mRNA whose translation is upregulated in response to increased concentrations of iron. Finally, we demonstrate FLARIM in mouse hippocampal neurons, in which local translation of mRNA in the neuronal processes is essential to cell growth and development. We first demonstrate FLARIM in neurons using probes for β-actin mRNA. We then show that FLARIM detects increased transcription and translation of activity regulated cytoskeletal protein (Arc) mRNA in response to neuronal activation with brain-derived neurotrophic factor (BDNF). We also compare the cellular distribution between the major microtubule-associated protein 2 (MAP2) mRNA isoforms, whose translation will be characterized in future FLARIM experiments. Overall, this work expands the capability of smFISH to study mRNA translation in addition to transcription, and it

shows the utility of *in situ* translation analysis in characterizing single-cell gene expression.

PUBLISHED CONTENT AND CONTRIBUTIONS

Burke, K.S., Antilla, K.A., Tirrell, D.A. "A fluorescence in situ hybridization method to quantify mRNA translation by visualizing ribosome-mRNA interactions in single cells." *ACS Central Science*, 2017, DOI: 10.1021/acscentsci.7b00048

K.S. Burke and D.A. Tirrell participated in conception of the project. K.S. Burke and K.A. Antilla completed experimental work and data analysis. K.S. Burke, K.A. Antilla, and D.A. Tirrell participated in writing of the manuscript.

TABLE OF CONTENTS

LIST OF ILLUSTRATIONS

Number *Page*

LIST OF TABLES

Number *Page*

NOMENCLATURE

CDS. Coding sequence.

FLARIM. Fluorescence assay to detect ribosome interactions with mRNA.

HCR. Hybridization chain reaction.

mRNA. Messenger RNA.

rRNA. Ribosomal RNA.

smFISH. Single-molecule fluorescence *in situ* hybridization.

smHCR. Single-molecule hybridization chain reaction.

UTR. Untranslated region.

β-actin. Beta Actin.

FTH1. Ferritin Heavy Chain.

Arc. Activity-regulated Cytoskeleton-associated Protein.

MAP2. Microtubule Associated Protein 2

Chapter 1

INTRODUCTION

1.1 Regulation of mRNA Translation

Translation, the process by which ribosomes synthesize protein from an mRNA transcript, is tightly regulated in cells to ensure that proteins are produced at the right time and in the right place. In eukaryotes, translation occurs in the cytoplasm and is carried out by the ribosome, which consists of two subunits composed of RNA and protein: the small subunit (40S) and the large subunit (60S). The small subunit of the mammalian ribosome contains one RNA species (the 18S ribosomal RNA (rRNA)) and 33 proteins. The large subunit of the mammalian ribosome contains three RNA species (28S, 5.8S, and 5S rRNA) and 47 proteins[1].

Translation is divided into three major steps: initiation, elongation, and termination. During initiation, specific protein factors and a methionyl transfer RNA (Met-tRNA) first bind to the 40S subunit to form a 40S preinitiation complex that then associates with mRNA. The preinitiation complex binds to a methylated guanine (called the 5' cap) in the 5' untranslated region (5' UTR) of most mRNAs[2]. However, for certain mRNAs and environmental conditions, the preinitiation complex can bind to an internal ribosomal entry site (IRES)[3] instead of the 5' cap. After binding, the preinitiation complex scans down the mRNA transcript in the 5' to 3' direction to reach the initiator codon, which is the nucleotide sequence AUG. The preinitiation complex pauses and the 60S subunit joins to form the 80S initiation complex, which carries out the elongation process. During elongation, the 80S ribosome scans the mRNA one codon at a time to build the nascent polypeptide chain. At each codon, a tRNA with a complementary anticodon sequence binds. This tRNA carries a specific amino acid, which forms a peptide bond (catalyzed by the peptidyl transferase center in the 60S subunit) with the amino acid on the previous tRNA. The cycle of tRNA binding and peptide bond formation continues until the full polypeptide is

synthesized. Termination of translation occurs when the 80S ribosome reaches the termination codon, which is not recognized by any tRNA. Instead, a release factor binds to the stop codon and promotes disassembly of the ribosome and mRNA complex to ultimately release the final protein product[2].

Translation is regulated both spatially and temporally by localizing mRNAs to specific subcellular compartments and translating those mRNAs into functional protein at the appropriate time(s). This regulation allows cells to respond rapidly to their environment, and it controls important biological processes including embryonic development[4], cell growth and migration[5], cell stress[6], and memory formation[7]. For example, early oogenesis and embryogenesis in *Drosophila* requires proper subcellular localization and subsequent translation of bicoid, nanos, oskar, and gurken mRNAs in the oocyte[8]. In *Xenopus*, asymmetric distribution of specific mRNAs in the oocyte establishes the body plan for the embryo and is critical to normal development[9]. In addition to organismal development, translational regulation is important to trigger cell stress responses and cell movement. During the unfolded protein response (UPR) in cells, several mRNAs are selectively upregulated in translation while the majority are downregulated[10,11]. In particular, activating transcription factor 4 (ATF4) mRNA switches from a translationally silent state to a highly active state without changes in its mRNA level during cell stress through a mechanism in which ribosomes are able bypass an inhibitory upstream open reading frame (uORF) in the transcript[12]. One of the most well characterized mRNAs that undergoes local translation to control cell growth and motility is Beta-actin (β-actin), which localizes to the leading edge of several different cell types. For instance, in chicken embryo fibroblasts, β-actin mRNA localizes to lamellipodia, and inhibition of this localization results in reduced cell motility[13–15]. β-actin mRNA appears at cell adhesions in mouse fibroblasts as well, and cell movement is enhanced or reduced when β-actin is concentrated at or displaced from these adhesions, respectively[16]. β-actin mRNA also localizes to dendrites in neurons and is required for neurite growth[17,18]. In addition to β-actin, thousands of different mRNAs have been identified in dendrites and or axons[19], and translation in these compartments allows

neurons to respond to their local environment[20]. Multiple studies have reported that translation of specific mRNAs in dendrites or axons helps form memories[7,21,22]. One example mRNA is calcium/calmodulin-dependent protein kinase II alpha (CamKIIα). When the 3'UTR of CamKIIα is mutated such that the mRNA and protein are restricted to the soma instead of dendrites, mice demonstrate impaired spatial memory, fear conditioning, and object recognition memory[23]. Fully understanding the role of translational regulation in these and other biological phenomena requires techniques to detect and quantify mRNA translation in a cellular context.

1.2 Techniques to measure mRNA Translation

Transcription and translation of mRNA can be measured with both ensemble and single-cell techniques. Global mRNA transcription is most commonly measured using RNA sequencing (RNA-seq). With RNA-seq, RNA is isolated from homogenized cells or tissues and is converted into cDNA via reverse transcription. The cDNA fragments are then sequenced to determine the mRNA species that were expressed and their relative abundances[24]. Another common tool to measure global transcription is a DNA microarray, which consists of a solid surface containing discrete spots of single-stranded DNA probes. The sequence of the probes in each spot corresponds to a specific gene in the sample of interest[25]. The microarray can be designed to cover an entire genome[26]. To measure transcription, purified mRNA from cell or tissue samples is reverse transcribed into cDNA, fluorescently labeled, and added to the microarray. The cDNAs hybridize to their complementary DNA probes on the microarray, thereby producing a fluorescence readout at the microarray spots containing those probes. The fluorescence intensity of each spot provides a relative measure of mRNA expression level[25].

In order to measure mRNA translation at the ensemble level, methods to quantify ribosome association with mRNA have been developed. Two common methods are polysome fractionation and ribosome profiling. Polysome fractionation determines the translation efficiency of a particular mRNA, whereas ribosome

profiling determines which mRNAs in a sample are being actively translated. In polysome fractionation, ribosomes are separated into polysome and non-polysome fractions using sucrose density gradient centrifugation. The relative abundances of an mRNA in the polysome and non-polysome fractions is then measured via Northern blot or reverse transcription polymerase chain reaction (RT-PCR)[27]. In ribosome profiling, mRNA fragments bound by ribosomes are isolated and sequenced to identify which mRNAs are translated and the relative level of their translation, as well as to which mRNA regions ribosomes bind[28–30].

In addition to techniques that detect ribosome association with mRNA, methods to identify and quantify proteins in a sample can be used to assess translation levels. Traditional quantitative proteomics is performed with two-dimensional gel electrophoresis (2-DE) and or mass spectrometry (MS). 2-DE separates proteins in a sample by both their isoelectric points and molecular weights[31]. Once proteins have been separated, the resulting gel bands can be compared between samples to identify proteins that are more or less abundant. These proteins can be identified from gel databases, such as the Swiss 2D-PAGE database. More commonly, the proteins are excised from the gel, digested, and analyzed by MS. With MS, proteins from a sample are ionized and their mass-to-charge ratio is measured to identify individual proteins and quantify their abundance[32]. Stable isotope labeling by amino acids in cell culture (SILAC) and bioorthogonal noncanonical amino acid tagging (BONCAT) are additional MS-based proteomic methods that can detect differences in protein abundance between samples and identify newly synthesized proteins, respectively[33,34].

These ensemble methods to measure mRNA transcription and translation are valuable to understand genome-wide expression levels within a population of cells. However, because these methods require tissue homogenization and or cell lysis, they do not provide information about the subcellular localization of transcription and translation. They also do not measure differences in gene expression between individual cells in a heterogeneous population. Gaining insight into local gene regulation in single cells requires *in situ* methods.

Fluorescence *in situ* hybridization (FISH) is a widely used method to study mRNA expression in fixed cells and tissue samples. FISH utilizes fluorescently labeled oligonucleotides (either DNA or RNA) that hybridize a target mRNA sequence and thereby produce a fluorescent signal at the site of the mRNA. Traditional FISH probes are 200-600 nucleotides long. They are generated by vector expression or PCR followed by nick translation, in vitro transcription, or random-primed DNA synthesis to incorporate nucleotides bearing fluorescent tags into the probes[35]. Because the probes are relatively long and therefore have low target specificity, traditional FISH is often limited to longer, higher copy transcripts and results in a broad staining pattern in cells[36,37]. More recently, single molecule FISH (smFISH) has been developed to detect individual mRNAs inside single cells[38,39]. smFISH utilizes multiple short, single-stranded and singly-labeled DNA probes that hybridize to an mRNA of interest. Probes are generally 20 nt long, and up to 48 probes are designed per mRNA transcript. Single molecules of a target mRNA are then visible as diffraction-limited fluorescent spots under a fluorescence microscope[39]. Various methods such as hybridization chain reaction (HCR) and RNAscope can be used to enhance the brightness and specificity of smFISH signals[40,41]. Most recently, single-molecule hybridization chain reaction (smHCR) has been used to generate bright, robust signals for detection of mRNA in cultured cells as well as in thick tissue samples[42]. Compared to smFISH, which uses probes carrying a single fluorophore, smHCR uses probes containing a single-stranded initiator sequence that binds and opens fluorescently labeled DNA hairpins. These hairpins assemble into a fluorescent polymer, resulting in a bright fluorescent signal at the site of amplification.

FISH methods detect and quantify mRNA, but they do not indicate whether mRNAs are translated into functional protein or not. Antibody staining is a common approach to visualize proteins and quantify their relative abundance *in situ*[43,44], but this method does not provide a direct measure of translation. Global protein synthesis can be monitored *in situ* with puromycylation and fluorescent noncanonical amino acid tagging (FUNCAT). For puromycylation, cells are treated with a low

concentration of the tRNA analog puromycin, which is recognized by the ribosome and incorporated into nascent peptide chains. Cells are fixed, and the puromyclated peptides are labeled with a fluorescent anti-puromycin antibody[45,46]. Alternatively, puromycin conjugated with fluorophores is used[47]. FUNCAT follows a similar procedure but uses amino acid analogues instead of puromycin. Cells are treated with chemically modified amino acids, which are incorporated into newly synthesized proteins by the cells' endogenous protein synthesis machinery. Cells are fixed and the amino acid analogues are coupled to fluorophores to highlight the cellular locations and relative level of protein synthesis[48]. Puromycylation and FUNCAT can also be combined with the proximity ligation assay (PLA) to detect translation of specific proteins *in situ*[49,50].

Puromycylation and FUNCAT require fixed cells. To visualize translation in live cells, the cell-permeable biarsenical dyes FlAsh and ReAsh have been developed. These dyes become fluorescent when they covalently react with a tetracysteine peptide motif that is genetically encoded into a protein of interest[51,52]. However, labeling with FlAsh and ReAsh does not provide information about the protein's corresponding mRNA. More recent live-cell imaging techniques utilize dual labeling systems in which an mRNA is genetically tagged with RNA stem loops to which a fluorescently-labeled coat protein binds, and the interaction of the mRNA with ribosomes is detected by colocalization of a second label[53–55]. In addition, live-cell imaging methods that simultaneously detect an mRNA and its nascent polypeptide product have been developed. In these methods, a reporter mRNA contains stem loops to which a genetically-encoded fluorescent protein binds, and the mRNA's peptide contains epitope tags to which genetically-encoded fluorescent antibodies bind[56–60]. Colocalization of fluorescence signals from the mRNA and its nascent polypeptide indicates active translation of that mRNA. These methods provide single-molecule resolution of mRNA translation in single living cells. However, they are limited to reporter mRNAs rather than endogenous transcripts. They also require cloning that may not be feasible for all cell types and mRNAs of interest and may affect cellular behavior.

We sought to develop a method that monitors mRNA translation in single cells and addresses the limitations of these existing methods. We decided to utilize RNA *in situ* hybridization and the hybridization chain reaction in a manner that produces bright fluorescence when ribosomes are bound to an mRNA of interest in fixed cells. We termed our method FLARIM, for fluorescence assay to detect ribosome interactions with mRNA. In Chapter 2, we describe FLARIM in detail and characterize its performance in mouse fibroblast cells. We demonstrate that FLARIM detects changes in translation of specific mRNAs under different environmental conditions, and we speculate that FLARIM can provide insights about local mRNA translation, a well-known phenomenon in neurons. We then address this application in Chapter 3 by using FLARIM in primary mouse hippocampal neurons. We study the mRNAs for β-actin, activity-regulated cytoskeleton-associated protein (Arc), and microtubule-associated protein 2 (MAP2).

1.3 References

(1) Wilson, D. N.; Doudna Cate, J. H. The Structure and Function of the Eukaryotic Ribosome. *Cold Spring Harb. Perspect. Biol.* **2012**, *4*, 1–17 DOI: 10.1101/cshperspect.a011536.

(2) Hershey, J. W. B. Translational Control in Mammalian Cells. *Annu. Rev. Biochem.* **1991**, *60*, 717–755 DOI: 10.1146/annurev.bi.60.070191.003441.

(3) Martínez-Salas, E.; Piñeiro, D.; Fernández, N. Alternative Mechanisms to Initiate Translation in Eukaryotic mRNAs. *Comp. Funct. Genomics* **2012**, *2012* DOI: 10.1155/2012/391546.

(4) Curtis, D.; Lehmann, R.; Zamore, P. D. Translational Regulation in Development. *Cell* **1995**, *81*, 171–178 DOI: 10.1016/0092-8674(95)90325-9.

(5) Liao, G.; Mingle, L.; Van De Water, L.; Liu, G. Control of Cell Migration through mRNA Localization and Local Translation. *Wiley Interdiscip. Rev. RNA* **2015**, *6*, 1–15 DOI: 10.1002/wrna.1265.

(6) Holcik, M.; Sonenberg, N. Translational Control in Stress and Apoptosis. *Nat. Rev. Mol. Cell Biol.* **2005**, *6*, 318–327 DOI: 10.1038/nrm1618.

(7) Costa-mattioli, M.; Sossin, W. S.; Klann, E.; Sonenberg, N. Translational Control of Long-Lasting Synaptic Plasticity and Memory. *Neuron* **2009**, *61*, 10–26 DOI: 10.1016/j.neuron.2008.10.055.

(8) Johnstone, O.; Lasko, P. Translational Regulation and RNA Localization in Drosophila Oocytes and Embryos. *Annu. Rev. Genet.* **2001**, *35*, 365–406.

(9) King, M. Lou; Messitt, T. J.; Mowry, K. L. Putting RNAs in the Right Place at the Right Time: RNA Localization in the Frog Oocyte. *Biol. Cell* **2005**, *97*, 19–33 DOI: 10.1042/BC20040067.

(10) Kaufman, R. Regulation of mRNA Translation by Protein Folding in the Endoplasmic Reticulum. *Trends Biochem. Sci.* **2004**, *29*, 152–158 DOI: 10.1016/j.tibs.2004.01.004.

(11) Ventoso, I.; Kochetov, A.; Montaner, D.; Dopazo, J.; Santoyo, J. Extensive Translatome Remodeling during ER Stress Response in Mammalian Cells. *PLoS One* **2012**, *7*, 1–12 DOI: 10.1371/journal.pone.0035915.

(12) Vattem, K. M.; Wek, R. C. Reinitiation Involving Upstream ORFs Regulates ATF4 mRNA Translation in Mammalian Cells. *Proc. Natl. Acad. Sci. U. S. A.* **2004**, *101*, 11269–11274 DOI: 10.1073/pnas.0400541101.

(13) Lawrence, J. B.; Singer, R. H. Intracellular Localization of Messenger RNAs for Cytoskeletal Proteins. *Cell* **1986**, *45*, 407–415 DOI: 10.1016/0092-8674(86)90326-0.

(14) Kislauskis, E. H.; Zhu, X.; Singer, R. H. Beta-Actin Messenger RNA Localization and Protein Synthesis Augment Cell Motility. *J. Cell Biol.* **1997**, *136*, 1263–1270 DOI: 10.1083/jcb.136.6.1263.

(15) Shestakova, E. A.; Singer, R. H.; Condeelis, J. The Physiological Significance of β-Actin mRNA Localization in Determining Cell Polarity and Directional Motility. *Proc. Natl. Acad. Sci. U. S. A.* **2001**, *98*, 7045–7050 DOI: 10.1073/pnas.121146098.

(16) Katz, Z. B.; Wells, A. L.; Park, H. Y.; Wu, B.; Shenoy, S. M.; Singer, R. H. β-Actin mRNA Compartmentalization Enhances Focal Adhesion Stability and Directs Cell Migration. *Genes Dev.* **2012**, *26*, 1885–1890 DOI: 10.1101/gad.190413.112.

(17) Eom, T.; Antar, L. N.; Singer, R. H.; Bassell, G. J. Localization of a Beta-Actin Messenger Ribonucleoprotein Complex with Zipcode-Binding Protein Modulates the Density of Dendritic Filopodia and Filopodial Synapses. *J. Neurosci.* **2003**, *23*, 10433–10444 DOI: 0270-6474/03/2310433-12.

(18) Hüttelmaier, S.; Zenklusen, D.; Lederer, M.; Dictenberg, J.; Lorenz, M.; Meng, X.; Bassell, G. J.; Condeelis, J.; Singer, R. H. Spatial Regulation of β-Actin Translation by Src-Dependent Phosphorylation of ZBP1. *Nature* **2005**, *438*, 512–515 DOI: 10.1038/nature04115.

(19) Cajigas, J.; Tushev, G.; Will, T. J.; Dieck, S.; Fuerst, N.; Schuman, E. M. The Local Transcriptome in the Synaptic Neuropil Revealed by Deep Sequencing and High-Resolution Imaging. *Neuron* **2012**, *74*, 453–466 DOI: 10.1016/j.neuron.2012.02.036.

(20) Lin, A. C.; Holt, C. E. Local Translation and Directional Steering in Axons. *EMBO J.* **2007**, *26*, 3729–3736 DOI: 10.1038/sj.emboj.7601808.

(21) Davis, H. P.; Squire, L. R. Protein Synthesis and Memory: A Review. *Psychol. Bull.* **1984**, *96*, 518–559 DOI: 10.1037/0033-2909.96.3.518.

(22) Sutton, M. A.; Schuman, E. M. Dendritic Protein Synthesis, Synaptic Plasticity, and Memory. *Cell* **2006**, *127*, 49–58 DOI: 10.1016/j.cell.2006.09.014.

(23) Miller, S.; Yasuda, M.; Coats, J. K.; Jones, Y.; Martone, M. E.; Mayford, M.

Disruption of Dendritic Translation of CaMKIIalpha Impairs Stabilization of Synaptic Plasticity and Memory Consolidation. *Neuron* **2002**, *36*, 507–519 DOI: 10.1016/S0896-6273(02)00978-9.

(24) Mortazavi, A.; Williams, B. A.; McCue, K.; Schaeffer, L.; Wold, B. Mapping and Quantifying Mammalian Transcriptomes by RNA-Seq. *Nat. Methods* **2008**, *5*, 621–628 DOI: 10.1038/nmeth.1226.

(25) Schena, M.; Shalon, D.; Davis, R. W.; Brown, P. O. Quantitative Monitoring of Gene Expression Patterns with a Complementary DNA Microarray. *Science* **1995**, *270*, 467–470 DOI: 10.1126/science.270.5235.467.

(26) Bertone, P.; Stolc, V.; Royce, T. E.; Rozowsky, J. S.; Urban, A. E.; Zhu, X.; Rinn, J. L.; Tongprasit, W.; Samanta, M.; Weissman, S.; Gerstein, M.; Snyder, M. Global Identification of Human Transcribed Sequences with Genome Tiling Arrays. *Science* **2004**, *306*, 2242–2246 DOI: 10.1126/science.1103388.

(27) Gandin, V.; Sikström, K.; Alain, T.; Morita, M.; McLaughlan, S.; Larsson, O.; Topisirovic, I. Polysome Fractionation and Analysis of Mammalian Translatomes on a Genome-Wide Scale. *J. Vis. Exp.* **2014**, *87*, 1–10 DOI: 10.3791/51455.

(28) Ingolia, N. T.; Ghaemmaghami, S.; Newman, J. R. S.; Weissman, J. S. Genome-Wide Analysis in Vivo of Translation with Nucleotide Resolution Using Ribosome Profiling. *Science* **2009**, *324*, 218–223 DOI: 10.1126/science.1168978.

(29) Jan, C. H.; Williams, C. C.; Weissman, J. S. Principles of ER Cotranslational Translocation Revealed by Proximity-Specific Ribosome Profiling. *Science* **2014**, *346*, 1–8 DOI: 10.1126/science.1257521.

(30) Williams, C. C.; Jan, C. H.; Weissman, J. S. Targeting and Plasticity of Mitochondrial Proteins Revealed by Proximity-Specific Ribosome Profiling. *Science* **2014**, *346*, 748–751 DOI: 10.1126/science.1257522.

(31) Rabilloud, T.; Lelong, C. Two-Dimensional Gel Electrophoresis in Proteomics: A Tutorial. *J. Proteomics* **2011**, *74*, 1829–1841 DOI: 10.1016/j.jprot.2011.05.040.

(32) Yates, J. R.; Ruse, C. I.; Nakorchevsky, A. Proteomics by Mass Spectrometry: Approaches, Advances, and Applications. *Annu. Rev. Biomed. Eng.* **2009**, *11*, 49–79 DOI: 10.1146/annurev-bioeng-061008-124934.

(33) Ong, S. Stable Isotope Labeling by Amino Acids in Cell Culture, SILAC, as

a Simple and Accurate Approach to Expression Proteomics. *Mol. Cell. Proteomics* **2002**, *1*, 376–386 DOI: 10.1074/mcp.M200025-MCP200.

(34) Dieterich, D. C.; Link, A. J.; Graumann, J.; Tirrell, D. A.; Schuman, E. M. Selective Identification of Newly Synthesized Proteins in Mammalian Cells Using Bioorthogonal Noncanonical Amino Acid Tagging (BONCAT). *Proc. Natl. Acad. Sci. U. S. A.* **2006**, *103*, 9482–9487 DOI: 10.1073/pnas.0601637103.

(35) Morrison, L. E.; Ramakrishnan, R.; Ruffalo, T. M.; Wilber, K. A. Labeling Fluorescence In Situ Hybridization Probes for Genomic Targets. In *Methods in Molecular Biology, Vol 204: Molecular Cytogenetics: Protocols and Applications*; 2003; Vol. 204, pp 21–40.

(36) Levsky, J. M.; Singer, R. H. Fluorescence in Situ Hybridization: Past, Present and Future. *J. Cell Sci.* **2003**, *116*, 2833–2838 DOI: 10.1242/jcs.00633.

(37) Singer, R. H.; Ward, D. C. Actin Gene Expression Visualized in Chicken Muscle Tissue Culture by Using in Situ Hybridization with a Biotinated Nucleotide Analog. *Proc. Natl. Acad. Sci. U. S. A.* **1982**, *79*, 7331–7335 DOI: 10.1073/pnas.79.23.7331.

(38) Raj, A.; Peskin, C. S.; Tranchina, D.; Vargas, D. Y.; Tyagi, S. Stochastic mRNA Synthesis in Mammalian Cells. *PLoS Biol.* **2006**, *4*, 1707–1719 DOI: 10.1371/journal.pbio.0040309.

(39) Raj, A.; Bogaard, P. Van Den; Rifkin, S. A.; Oudenaarden, A. Van; Tyagi, S. Imaging Individual mRNA Molecules Using Multiple Singly Labeled Probes. *Nat. Methods* **2008**, *5*, 877–879 DOI: 10.1038/NMETH.1253.

(40) Choi, H. M. T.; Beck, V. A.; Pierce, N. A. Next-Generation in Situ Hybridization Chain Reaction : Higher Gain , Lower Cost , Greater Durability. *ACS Nano* **2014**, *8*, 4284–4294 DOI: 10.1021/nn405717p C2014.

(41) Wang, F.; Flanagan, J.; Su, N.; Wang, L. C.; Bui, S.; Nielson, A.; Wu, X.; Vo, H. T.; Ma, X. J.; Luo, Y. RNAscope: A Novel in Situ RNA Analysis Platform for Formalin-Fixed, Paraffin-Embedded Tissues. *J. Mol. Diagnostics* **2012**, *14*, 22–29 DOI: 10.1016/j.jmoldx.2011.08.002.

(42) Shah, S.; Lubeck, E.; Schwarzkopf, M.; He, T.; Greenbaum, A.; Sohn, C. H.; Lignell, A.; Choi, H. M. T.; Gradinaru, V.; Pierce, N. A.; Cai, L. Single-Molecule RNA Detection at Depth via Hybridization Chain Reaction and Tissue Hydrogel Embedding and Clearing. *Development* **2016**, *143*, 2862–2867 DOI: 10.1242/dev.138560.

(43) Beutner, E. H. Immunofluorescent Staining: The Fluorescent Antibody Method. *Bacteriol. Rev.* **1961**, *25*, 49–76.

(44) Ramos-Vara, J. A. Technical Aspects of Immunohistochemistry. *Vet. Pathol.* **2005**, *42*, 405–426 DOI: 10.1354/vp.42-4-405.

(45) Schmidt, E. K.; Clavarino, G.; Ceppi, M.; Pierre, P. SUnSET, a Nonradioactive Method to Monitor Protein Synthesis. *Nat. Methods* **2009**, *6*, 275–277 DOI: 10.1038/nmeth.1314.

(46) David, A.; Dolan, B. P.; Hickman, H. D.; Knowlton, J. J.; Clavarino, G.; Pierre, P.; Bennink, J. R.; Yewdell, J. W. Nuclear Translation Visualized by Ribosome-Bound Nascent Chain Puromycylation. *J. Cell Biol.* **2012**, *197*, 45–57 DOI: 10.1083/jcb.201112145.

(47) Starck, S. R.; Green, H. M.; Alberola-Ila, J.; Roberts, R. W. A General Approach to Detect Protein Expression In Vivo Using Fluorescent Puromycin Conjugates. *Chem. Biol.* **2004**, *11*, 999–1008 DOI: 10.1016/j.chembiol .2004.05.011.

(48) Dieterich, D. C.; Hodas, J. J. L.; Gouzer, G.; Shadrin, I. Y.; Ngo, J. T.; Triller, A.; Tirrell, D. A.; Schuman, E. M. In Situ Visualization and Dynamics of Newly Synthesized Proteins in Rat Hippocampal Neurons. *Nat. Neurosci.* **2010**, *13*, 897–905 DOI: 10.1038/nn.2580.

(49) Söderberg, O.; Gullberg, M.; Jarvius, M.; Ridderstråle, K.; Leuchowius, K.-J.; Jarvius, J.; Wester, K.; Hydbring, P.; Bahram, F.; Larsson, L.-G.; Landegren, U. Direct Observation of Individual Endogenous Protein Complexes in Situ by Proximity Ligation. *Nat. Methods* **2006**, *3*, 995–1000 DOI: 10.1038/nmeth947.

(50) tom Dieck, S.; Kochen, L.; Hanus, C.; Heumüller, M.; Bartnik, I.; Nassim-Assir, B.; Merk, K.; Mosler, T.; Garg, S.; Bunse, S.; Tirrell, D. A.; Schuman, E. M. Direct Visualization of Newly Synthesized Target Proteins in Situ. *Nat. Methods* **2015**, *12*, 411–414 DOI: 10.1038/nmeth.3319.

(51) Griffin, B. A.; Adams, S. R.; Tsien, R. Y. Specific Covalent Labeling of Recombinant Protein Molecules Inside Live Cells. *Science* **1998**, *281*, 269–272 DOI: 10.1126/science.281.5374.269.

(52) Machleidt, T.; Robers, M.; Hanson, G. T. Protein Labeling With FlAsH and ReAsH. In *Methods in Molecular Biology, vol. 356: High Content Screening: A Powerful Approach to Systems Cell Biology and Drug Discovery*; Humana Press, Inc.: Totowa, NJ, 2007; Vol. 356, pp 209–220.

(53) Halstead, J. M.; Lionnet, T.; Wilbertz, J. H.; Wippich, F.; Ephrussi, A.; Singer, R. H.; Chao, J. A. An RNA Biosensor for Imaging the First Round of Translation from Single Cells to Living Animals. *Science* **2015**, *347*, 1367–1370 DOI: 10.1126/science.aaa3380.

(54) Wu, B.; Buxbaum, A. R.; Katz, Z. B.; Yoon, Y. J.; Singer, R. H. Quantifying Protein-mRNA Interactions in Single Live Cells. *Cell* **2015**, *162*, 211–220 DOI: 10.1016/j.cell.2015.05.054.

(55) Katz, Z. B.; English, B. P.; Lionnet, T.; Yoon, Y. J.; Monnier, N.; Ovryn, B.; Bathe, M.; Singer, R. H. Mapping Translation "Hot-Spots" in Live Cells by Tracking Single Molecules of mRNA and Ribosomes. *eLife* **2016**, *5*, e10415 DOI: 10.7554/eLife.10415.

(56) Morisaki, T.; Lyon, K.; Deluca, K. F.; Deluca, J. G.; English, B. P.; Lavis, L. D.; Grimm, J. B.; Viswanathan, S.; Looger, L. L.; Lionnet, T.; Stasevich, T. J. Real-Time Quantification of Single RNA Translation Dynamics in Living Cells. *Science* **2016**, *899*, 1–10 DOI: 10.1126/science.aaf0899.

(57) Wang, C.; Han, B.; Zhou, R.; Zhuang, X. Real-Time Imaging of Translation on Single mRNA Transcripts in Live Cells. *Cell* **2016**, *165*, 990–1001 DOI: 10.1016/j.cell.2016.04.040.

(58) Wu, B.; Eliscovich, C.; Yoon, Y. J.; Singer, R. H. Translation Dynamics of Single mRNAs in Live Cells and Neurons. *Science* **2016**, *1084*, 1–10 DOI: 10.1126/science.aaf1084.

(59) Yan, X.; Hoek, T. A.; Vale, R. D.; Tanenbaum, M. E. Dynamics of Translation of Single mRNA Molecules In Vivo. *Cell* **2016**, *165*, 976–989 DOI: 10.1016/j.cell.2016.04.034.

(60) Pichon, X.; Bastide, A.; Safieddine, A.; Chouaib, R.; Samacoits, A.; Basyuk, E.; Peter, M.; Mueller, F.; Bertrand, E. Visualization of Single Endogenous Polysomes Reveals the Dynamics of Translation in Live Human Cells. *J. Cell Biol.* **2016**, *214*, 769–781 DOI: 10.1083/jcb.201605024.

C h a p t e r 2

USING FLUORESCENCE *IN SITU* HYBRIDIZATION TO QUANTIFY MRNA TRANSLATION IN SINGLE CELLS

Published as:

Burke, K.S., Antilla, K.A., Tirrell, D.A. "A fluorescence in situ hybridization method to quantify mRNA translation by visualizing ribosome-mRNA interactions in single cells." *ACS Central Science*, 2017, DOI: 10.1021/acscentsci.7b00048

2.1 Summary

Precise spatiotemporal control of mRNA translation is critical for regulating cellular processes. Single-molecule detection of mRNA via fluorescence *in situ* hybridization (FISH) has revealed when specific mRNAs are produced and where they are located in cells. However, current FISH methods cannot determine when and where these single molecules of mRNA are translated into protein. While live-cell imaging techniques have been developed to track when an mRNA associates with ribosomes or produces its peptide product, these techniques require genetic manipulation that may be difficult and time-consuming to accomplish. In addition, the methods are not applicable to fixed samples. We sought to develop a simple, inexpensive method to visualize and quantify changes in mRNA translation in fixed cells. Our method – termed FLARIM, for fluorescence assay to detect ribosome interactions with mRNA – utilizes RNA *in situ* hybridization and the hybridization chain reaction to produce bright fluorescence when ribosomes are bound to an mRNA of interest. FLARIM is applicable to any endogenous mRNA in cells and does not involve any structural or genetic perturbations. We demonstrate that FLARIM effectively detects changes in mRNA translation of specific genes under different environmental conditions. FLARIM also inherently measures mRNA transcription, thereby providing greater insight into two fundamental processes of gene expression.

2.2 Introduction

Gene expression is regulated at both the transcriptional and translational levels. For many genes, changes in mRNA and protein levels are not correlated[1–4], and protein abundance is often dominated by translation rather than transcription[5]. Translational regulation is necessary to coordinate the timing, amount, and location of protein synthesis, and is essential to biological processes including cell morphogenesis and migration[6,7], organismal development[8], responses to cell stress[9], and memory formation[10].

Ensemble biochemical methods are widely used to measure global changes in mRNA transcription and translation in cells. The most common method for transcriptomic analysis is RNA-seq[11]. Ribosome profiling is an extension of RNA-seq in which mRNA fragments bound by ribosomes are isolated and sequenced to assess mRNA translation[3,12,13]. The translation efficiency of a particular mRNA can also be determined by fractionating ribosomes using sucrose density gradient centrifugation and measuring the relative abundances of the mRNA in the polysome and non-polysome fractions[14]. These methods measure genome-wide expression levels in populations of cells (although RNA-seq has been modified to measure mRNA expression in single cells as well[15]). Because these methods require cell disruption, they provide no information about subcellular localization of transcription and translation for particular genes. In order to study local gene regulation, *in situ* methods that detect mRNA and protein within cells are required.

Various *in situ* fluorescence imaging techniques have been developed to study transcription and translation in single cells with spatial and temporal resolution[16]. Transcription is commonly measured with single-molecule fluorescence *in situ* hybridization (smFISH), in which mRNAs are probed with fluorophore-labeled DNA oligonucleotides so that their numbers and locations in single cells can be quantified. Several methods have been developed to enhance the brightness and specificity of smFISH[17,18]. Recently, the single-molecule hybridization chain reaction (smHCR) has been developed to achieve bright, robust signals for detection of mRNA in cultured cells as well as in thick tissue samples[19]. Changes in protein

translation can be measured via ^{35}S-methionine labeling[20], bioorthogonal non-canonical amino acid tagging (BONCAT)[21,22] or puromycylation[23–25]. The latter methods can be combined with the proximity ligation assay (PLA)[26] to detect translation of specific proteins *in situ*[27], but none of these approaches provides information about mRNA abundance or location.

Live-cell fluorescence imaging techniques have utilized dual labeling systems in which an mRNA is genetically tagged with stem-loop recognition elements (MS2 or PP7 stem loops) to which a fluorescently-labeled coat protein binds, and the interaction of the mRNA with ribosomes is detected by colocalization of a second label[28–30]. Recently, multiple live-cell imaging methods have been developed to simultaneously detect an mRNA and its nascent polypeptide product. Here, a reporter mRNA contains MS2 or PP7 stem loops and the nascent polypeptide encodes an array of epitope tags to which genetically-encoded fluorescent antibodies bind[31–35]. Colocalization of fluorescence signals from an mRNA and its nascent polypeptide indicates active translation of that mRNA. These methods are the first to provide single-molecule resolution of mRNA translation events in single living cells. However, they are limited to monitoring reporter mRNAs rather than endogenous transcripts. The cloning required to implement these methods may affect cellular behavior and may not be feasible for all cell types and mRNAs of interest.

We have developed an imaging method that uses RNA *in situ* hybridization and the hybridization chain reaction (HCR) to probe translation of unmodified endogenous mRNA transcripts in single fixed cells (Figure 1A). We call this method FLARIM, for fluorescence assay to detect ribosome interactions with mRNA. FLARIM reveals interactions between individual mRNAs and ribosomes to provide a measure of the extent of active translation of the target mRNA species. The method does not require genetic manipulation of cells and can be applied to almost any mRNA of interest. As ribosome profiling extends RNA-seq to quantify mRNAs bound by ribosomes, FLARIM extends smFISH to identify ribosome-bound mRNAs and to monitor the changes in ribosome-mRNA interaction that accompany cellular

perturbations. Because FLARIM yields images of fixed cells, the subcellular locations where mRNAs interact with ribosomes can be determined.

Here we introduce and characterize FLARIM in NIH 3T3 mouse fibroblasts. We first demonstrate the method by detecting the interaction of β-actin mRNA with ribosomes, and by probing how this interaction changes upon treatment with the translation inhibitor puromycin. Both the fraction of mRNAs bound to ribosomes and the intensities of individual interaction signals decrease. We then examine translational regulation of ferritin heavy chain (FTH1) mRNA in response to added iron. We observe an increase in ribosome-mRNA interaction over a 24-h iron incubation period. We also note a small increase in FTH1 mRNA copy number for cells treated with iron, in contrast to previous reports that FTH1 mRNA levels are unchanged by addition of iron[36,37]. FLARIM thus provides both spatial and temporal information about two of the key steps in regulation of gene expression.

2.3 Results and Discussion

To visualize ribosome-bound mRNAs, we use pairs of oligonucleotide probes that bind separately to ribosomes (via ribosomal RNA) and to the mRNA of interest, and that produce strong fluorescence signals via the hybridization chain reaction (HCR) when in close proximity (Figure 2.1A). Ribosomes are hybridized with multiple oligonucleotide probes that bind to 18S ribosomal RNA (rRNA). We used the mouse rRNA secondary structure of Holmberg *et al.*[38] to identify regions on the 18S rRNA that are relatively unstructured and that contain bases shown to be accessible for chemical modification. We preferentially targeted our ribosome probes to these regions and designed 24 unique probes in total. We verified that the corresponding sense probes for 18S rRNA do not produce fluorescence via FISH (Figure 2.S1). An mRNA of interest is hybridized with two different sets of oligonucleotide probes: one (designated “mRNA interaction probes”) that pairs with the ribosome probes to form binding sites for a linker probe that carries an HCR initiator, and a second (“mRNA transcript probes”) that separately labels the mRNA transcript with a different HCR initiator. Interaction probes are targeted to the coding

sequence (CDS), the region of the mRNA that is translated by ribosomes. Transcript probes are primarily targeted to untranslated regions (5'UTR and 3'UTR) of the mRNA. We targeted each mRNA region with 15 - 36 probes. Multiple probes are used per target in order to increase the signal to noise ratio and to discriminate signal arising from true mRNAs from signal resulting from nonspecific binding of individual probes[39,40]. Sequences of all oligonucleotide probes used in this study are listed in Supplemental Table 1.

Each mRNA transcript probe contains an HCR initiator sequence and a 25-nucleotide (nt) region complementary to the mRNA. In HCR, a single-stranded initiator sequence is used to bind and open fluorescently labeled DNA hairpins that then assemble into a fluorescent polymer, resulting in a bright fluorescent signal at the site of amplification. Choi and coworkers have introduced five unique HCR initiator sequences (designated B1-B5), each with a corresponding pair of HCR hairpins for fluorescence amplification[17]. We used the B2 HCR initiator and its corresponding hairpins coupled to Alexa Fluor 488 for all mRNA transcript probes (Figure S2, Table S1). Each mRNA interaction probe and each ribosome probe contains a 25-nt region complementary to its target RNA, a 13-nt polyA spacer, and a 22-nt extension sequence. A common extension sequence is used for all mRNA interaction probes, and a different extension sequence is used for all ribosome probes (Figure 2.S2, Table 2.S1).

Extension sequences on the mRNA interaction and ribosome probes are hybridized with an oligonucleotide linker probe bearing a 26-nt binding sequence that spans both extensions when they are in close proximity (15 nt hybridize to the mRNA extensions; 11 nt hybridize to the ribosome extensions) (Figure 2.S2). The binding strength of the linker is tuned with formamide, which lowers the melting temperature of DNA[41]. The amount of formamide in solution during the linker hybridization step and subsequent wash steps is adjusted such that the linker remains bound when it spans both extension sequences but not when it hybridizes only one extension (Figure 1A). We determined the appropriate amount of formamide by titrating it in our wash solution and our hybridization buffer during the linker

hybridization step. We found that 35% formamide removed the most background signal without comprising hybridization of mRNA transcript probes (Figure 2.S3).

The linker probe also contains an HCR initiator sequence. We used the B3 HCR initiator and its corresponding HCR hairpins coupled to Alexa Fluor 546 to amplify fluorescence signals associated with the linker probe. Signals from the linker probes and from mRNA transcript probes appear as single, diffraction-limited spots when visualized by confocal microscopy (Figure 2.1C). In the ideal FLARIM scheme, spots that colocalize in the Alexa 488 (shown in red throughout this study) and Alexa 546 (shown in green throughout this study) channels indicate mRNAs bound to ribosomes; spots that appear only in the Alexa 488 channel indicate mRNAs that do not interact with ribosomes. On the basis of the assumption that three nucleotides add ~1 nm to the length of a DNA probe[42], we estimated that ribosome probes and mRNA interaction probes must be separated by no more than ~18 nm if they are to produce interaction signals.

We first tested FLARIM *in situ* in NIH 3T3 fibroblasts, using probes designed for β-actin mRNA. Control experiments in which either the mRNA interaction probes or the ribosome probes were omitted showed little or no labeling from the linker probe, consistent with our expectation that the linker can be effectively washed out of cells when it binds only to an mRNA interaction probe or to a ribosome probe. However, when both probe sets were present, we saw a significant increase in signal from the linker probe (Figure 2.1B) and substantial colocalization of these signals with those derived from the β-actin transcript probes (Figure 2.1C). We found on average that 61 ± 4% (n = 21 cells) of β-actin transcripts in the cytoplasm were colocalized with ribosomes.

We examined β-actin transcript probes in control experiments with either ribosome probes or mRNA interaction probes to ensure that signals from the combination of the latter two probe sets showed significantly higher colocalization to β-actin transcripts than to background signals from either probe set alone. Both sets of HCR hairpins were added to all control experiments. Samples with ribosome probes or mRNA interaction probes alone produced punctate Alexa 546 emission to

which only 8 ± 1% (n = 10 cells) and 7 ± 2% (n = 11 cells) of Alexa 488 spots colocalized, respectively (Figure 2.1D, Table 2.S3). We also checked potential background colocalization from the linker probe. Cells treated with the linker probe alone produced spots of Alexa 546 emission that colocalized to fewer than 1% (n = 11 cells) of Alexa 488 spots (Table 2.S3). We conclude that the levels of false positive signals arising from nonspecific binding of the linker, or from the HCR amplification step, are low. As a further check on the method, we analyzed ribosome interaction with β-actin mRNA in cell nuclei, where translation is not expected to occur. We found that only 12 ± 12% (n = 10 cells) of β-actin transcripts in cell nuclei colocalized with ribosome signal, consistent with the results of the control experiments described above (Figure 2.S4). The uncertainty in the measurement of nuclear colocalization arises from the small number (average of 11 ± 4 spots per nucleus for 10 cells) of β-actin mRNA spots in the nucleus. To determine the utility of FLARIM for the study of transcripts characterized by lower copy numbers, we examined Actin-related protein 3 (Arp3) mRNA, which is ~10X less abundant than β-actin mRNA (we measured an average of 190 Arp3 mRNAs per cell, n = 31 cells). As with β-actin, we found that the fraction Arp3 transcripts that colocalized to background signal from ribosome or mRNA interaction probes alone was at least 8X lower than the fraction that colocalized to signal from the combination of both probe sets (Figure 2.S5).

The percentage of cytoplasmic β-actin transcripts observed to bind ribosomes (61 ± 4%) is almost certainly an underestimate. Fluorescence signals generated by smFISH and smHCR invariably yield less than 100% colocalization for probes targeted to the same message[19,39,43]. For example, Shah and coworkers found that when using three sets of smHCR probes per transcript, approximately 85% of spots from a single channel colocalized with spots from at least one other channel[19]. To set an upper bound on the extent of ribosome-mRNA interaction to be expected in our β-actin experiments, we performed another control experiment in which we replaced the linker probe (which hybridizes to only 15 nt of the mRNA interaction probe) with a linker complementary to 24 nt of the interaction probe (see Figure 2.S6 schematic).

This experiment showed 74 ± 3% of Alexa 488 spots to colocalize with spots in the Alexa 546 channel (Figure 2.S6). This result indicates that the measured value of 61 ± 4% is indeed an underestimate of the percent of cytoplasmic β-actin transcripts bound to ribosomes. Our results are consistent with the polysome profiling data of Ventoso and coworkers, who found the fraction of β-actin mRNAs associated with polysomes in NIH 3T3 cells to be 0.72[44].

We tested the sensitivity of FLARIM to changes in ribosome-mRNA binding by treating cells with puromycin, a translation inhibitor that causes dissociation of ribosomal subunits from mRNA[45]. The effect of puromycin is apparent in a comparison of side-by-side images of treated and untreated cells (Figure 2.2A). Cells treated with puromycin show less colocalization (yellow) between transcript spots (red) and ribosome-mRNA interaction spots (green). The percentage of β-actin transcripts interacting with ribosomes in the cytoplasm decreased from 61 ± 4% in control cells to 38 ± 6% in puromycin-treated cells (Figure 2.2B). Furthermore, the intensities of the fluorescence signals associated with single ribosome-mRNA interaction spots shifted to lower values (Figure 2.2C), indicating a reduction in the number of ribosomes bound per β-actin transcript.

The observed changes in signal colocalization and signal intensity with puromycin treatment demonstrate the sensitivity of the FLARIM method to perturbations in ribosome association with mRNA. We found no change in the average number of β-actin mRNAs per cell after puromycin treatment (Figure 2.S7). We measured an average of ~2000 β-actin transcripts per cell, in agreement Schwanhäusser's estimate of ~2200 β-actin transcripts per NIH 3T3 cell, as determined by mRNA sequencing[5]. We also found no change in the fraction of ribosome-mRNA interaction spots colocalizing with β-actin transcript spots after puromycin treatment (Table 2.S5). To estimate the total change in ribosome interaction with β-actin mRNA after puromycin treatment, we multiplied the fraction of β-actin mRNAs colocalized with ribosomes by the average intensity of the associated Alexa 546 spots. Since multiple mRNA interaction probes are used, a decrease in ribosome association with mRNA could result in fewer of these probes

per mRNA forming a successful interaction with ribosomes. A ribosome-mRNA interaction signal could still be produced, but it would have a lower fluorescence intensity. We observed a 2.6-fold decrease in ribosome interaction based on this metric (average of two independent experiments, n = 7-16 cells per condition per experiment). As an additional check on the sensitivity of FLARIM measurements to changes in ribosome association with mRNA, we treated cells with both puromycin and 4E1RCat, which inhibits formation of the translation initiation complex and hence prevents recruitment of the small ribosomal subunit to mRNA[46]. The percentage of β-actin transcripts interacting with ribosomes in this experiment dropped to 23 ± 5% (Figure 2.S8), indicating that the signal observed with puromycin treatment alone may have reflected binding of the small ribosomal subunit to the 5' UTR of β-actin mRNA.

We subjected the FLARIM method to a second test by examining the translational regulation of ferritin synthesis in response to iron treatment[47]. Under standard conditions in cell culture, ferritin heavy chain (FTH1) mRNA is translationally repressed by binding of an iron regulatory protein (IRP) to an iron response element (IRE) in the 5'UTR. Upon addition of iron, the IRP is released from the IRE, ribosomes bind to the mRNA, and FTH1 is efficiently translated[5,48,49] (Figure 2.3A). Increases in FTH1 protein levels in mammalian cells in response to elevated iron are attributed to increased translation (not transcription), as the levels of FTH1 mRNA have been shown to remain constant[36,37].

We used hemin, an iron porphyrin, as the source of iron. When added to cells in culture, hemin rapidly releases iron intracellularly, and has been shown to induce ferritin synthesis[36]. We added hemin at a final concentration of 50 μM to cell culture media and fixed cells after different periods of time. Western blotting confirmed that the FTH1 protein level increased upon addition of hemin (Figure 2.S9). In companion FLARIM experiments, we detected a noticeable increase in interaction of the FTH1 mRNA with ribosomes in cells treated with hemin (Figures 2.3B). After 4 h of treatment, the fraction of FTH1 mRNAs interacting with ribosomes per cell doubled, from 21 ± 4% in vehicle-treated cells to 43 ± 7% in cells incubated with hemin. The

extent of increased interaction was essentially constant over 24 h (Figure 2.3C). The intensities of the fluorescence signals associated with single ribosome-mRNA interaction spots also shifted to higher values (Figure 2.3D, Figure 2.S10). We found no significant colocalization of FTH1 transcript signals to background signals in control experiments containing only ribosome probes or only mRNA interaction probes (Table 2.S4). We also found no difference in the fraction of ribosome-mRNA interaction spots colocalizing with FTH1 transcript spots between vehicle-treated and iron-treated cells (Table 2.S6).

As discussed previously with respect to β-actin, FLARIM almost certainly provides underestimates of the fractions of ribosome-bound transcripts, owing to imperfect colocalization of the mRNA transcript and interaction probes (Figure 2.S6). Nevertheless, the method reveals distinct increases in ribosome association with FTH1 when translation of the mRNA is upregulated. Our finding that FTH1 transcripts are translated at a lower rate than β-actin transcripts is consistent with the polysome profiling data reported by Ventoso *et al.,* who found that only about 6% of FTH1 mRNAs are associated with polysomes in NIH 3T3 cells in the absence of iron treatment[44].

As before, we estimated the change in ribosome interaction with FTH1 mRNA after addition of iron by multiplying the fraction of FTH1 mRNAs colocalized with ribosomes by the average intensity of the associated Alexa 546 spots for each treatment condition. After 4 h, 12 h, and 24 h of iron treatment, we observed 2.7-, 2.2-, and 2.3-fold increases, respectively, in ribosome interaction with FTH1 mRNA compared to the vehicle control (average of three independent experiments, n = 10-17 cells per condition per experiment).

We detected an average of ~1000 FTH1 transcripts per NIH 3T3 cell in our vehicle control condition. In comparison, Schwanhäusser *et al.* estimated ~2200 FTH1 transcripts per NIH 3T3 cell in media with no added iron[5]. Although several previous studies report that FTH1 mRNA levels in mammalian cells are unchanged upon iron treatment[36,37], we observed a slight but statistically significant ($P<0.0002$ at 4 h, $P<0.0001$ at 12 h and 24 h) increase in the number of FTH1 mRNAs per cell

after iron treatment (Figure 2.3E). On average, cells treated with iron for 4 – 24 h contained roughly 40% more copies of FTH1 mRNA than untreated cells. This modest increase in mRNA may not have been detectable with previous studies, which used northern blotting for quantification of FTH1 mRNA abundance[36,37]. The increase may also be a unique response in NIH 3T3 cells under our experimental conditions. Studies that suggest unchanged levels of FTH1 mRNA upon treatment with iron have focused on rat liver cells and transgenic mouse fibroblasts[36,37,50]. However, an investigation of Friend erythroleukemia cells (FLCs) found that FTH1 mRNA expression increased by up to 10-fold upon treatment with hemin[51]. The fact that FLARIM reveals changes in both mRNA interaction with ribosomes and mRNA copy number illustrates the utility of the method in assessing both translational and transcriptional control of gene expression in single cells.

2.4 Conclusions

This study shows that changes in ribosome association with endogenous, unmodified mRNAs can be imaged and quantified *in situ* using standard DNA oligonucleotide probes and HCR. We characterized this method, which we termed FLARIM, in NIH 3T3 mouse fibroblasts. We first measured ribosome-mRNA interactions for β-actin in single cells and detected a decrease in these interactions when cells were treated with the translation inhibitor puromycin. We observed no significant ribosome-mRNA interactions in cell nuclei, where translation is not expected to occur, although a few studies report conflicting evidence[24,52]. We also detected increased ribosome binding to FTH1 mRNA when cells were treated with iron, and surprisingly, we noted an increase in FTH1 mRNA levels in concert with the increase in ribosome interaction. Because FLARIM interrogates both transcriptional and translational processes, it has the potential to provide unique insights into the nature of gene regulation in single cells. Although FLARIM was applied only to mouse cells in this study, we designed a nearly identical set of ribosome probes for human 18S rRNA (Table 2.S2) to facilitate FLARIM studies in human cells.

FLARIM is simple and inexpensive, uses commercially available reagents and common laboratory equipment, and requires no genetic manipulation of the cells of interest. Experiments can be completed in 2-3 days from cell fixation to image collection and analysis. Compared to various proximity ligation assays[53,54], which could conceivably be adapted to analyze interactions between ribosomes and mRNA, FLARIM requires fewer steps and is enzyme-free, making it cheaper and easier to modify for different sample types. The method is also amenable to the study of fixed clinical samples, which are inaccessible to techniques that require cloning. We anticipate that FLARIM will be especially useful in studies of local mRNA translation. For example, neurons contain thousands of different mRNA transcripts in their dendrites and or axons[55], and FLARIM is well suited to the monitoring of changes in ribosomal association of these transcripts in response to external stimuli. In similar fashion, studies of local translation during embryonic development[56] should prove fruitful.

FLARIM should be applicable to essentially any mRNA of interest; however, it does require that the mRNA be efficiently hybridized with oligonucleotide probes. It is conceivable that short mRNAs may not bind a sufficient number of probes to produce reliable signals. Using a higher number of probes is known to improve the robustness of mRNA detection[39] and to increase the ratio of signal to autofluorescence[40], although the number of probes needed for reliable mRNA detection may depend on the target transcript. It is also important to note that FLARIM does not yield a numerically accurate measure of the number of mRNAs being translated in the cell. Rather, it provides an approximate measure of translation, useful for comparisons among samples, along with spatial information and a measure of mRNA copy number. We use ribosome interaction as a proxy for translation, but it is known that mRNAs can be bound by ribosomes without being translated, e.g. in the case of ribosome stalling[57].

It should be straightforward to modify the FLARIM method to enable studies of other molecular interactions in single cells. In addition to RNA-RNA interactions, protein-RNA and protein-protein interactions can be revealed by using antibodies

conjugated to DNA oligonucleotides or by using aptamer probes[58]. Interactions with DNA might be measured by combining the method with DNA FISH techniques. The method is designed in a manner that makes it highly tunable. In adapting the method to detect interactions between different molecular species and in different cell types, the probe sequences and the stringency of the wash buffer can easily be adjusted to lower background and ensure that HCR amplification occurs essentially only from interacting probe pairs. Probe sequences can also be engineered to increase or decrease the maximum distance between probes that allows for signal generation.

2.5 Acknowledgements

We thank the National Science Foundation Graduate Research Fellowship Program (NSF GRFP, grant number 1144469), the Rose Hills Foundation (Caltech SURF), the German Research Foundation (Grant No MI 1315/4), and the Programmable Molecular Technology Initiative of the Gordon and Betty Moore Foundation for support of this work. We thank H.M.T. Choi and N.A. Pierce for suggesting the use of a linker probe carrying an HCR initiator as a mechanism for selectively generating signal from cognate probe pairs colocalized by targets in the sample. We thank Florian Mueller for development of FISH-quant and the Broad Institute for development of Cell Profiler for image analysis. We thank Johannes Stegmaier and the Center for Advanced Methods in Biological Image Analysis at the Beckman Institute (CAMBIA) for adapting the XPIWIT software tool for analysis of nuclear transcripts. We thank Andres Collazo for assistance with the LSM 800 confocal microscope in the Biological Imaging Facility of the Beckman Institute at Caltech.

2.6 Figures

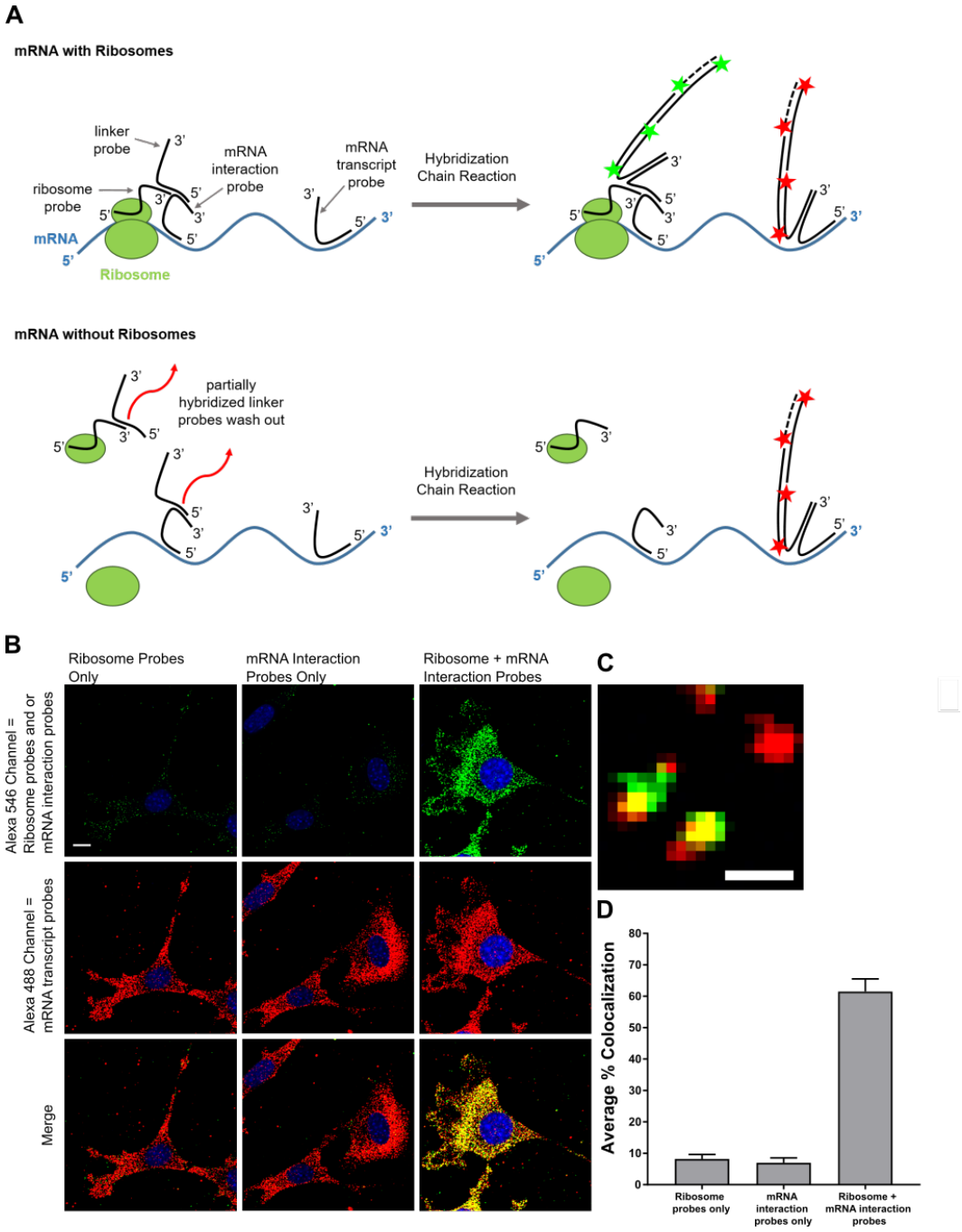
A
mRNA with Ribosomes
linker probe
ribosome probe
mRNA interaction probe
mRNA transcript probe
mRNA
Ribosome
Hybridization Chain Reaction
mRNA without Ribosomes
partially hybridized linker probes wash out
Hybridization Chain Reaction
B
Ribosome Probes Only
mRNA Interaction Probes Only
Ribosome + mRNA Interaction Probes
Alexa 546 Channel = Ribosome probes and or mRNA interaction probes
Alexa 488 Channel = mRNA transcript probes
Merge
C
D
Average % Colocalization
Ribosome probes only
mRNA interaction probes only
Ribosome + mRNA interaction probes

Figure 2.1 (*previous page*): Illustration of FLARIM. (A) Schematic of method to detect ribosome-mRNA interactions *in situ*. Multiple DNA oligonucleotide probes are hybridized to ribosomes via rRNA and two different mRNA regions. For illustration purposes, only a single probe per ribosome and mRNA region is shown. Top: When an mRNA is bound by ribosomes, the linker probe can hybridize across the extension sequences of both the ribosome probes and the mRNA interaction probes, and thereby produce a fluorescence signal via HCR. Bottom: When an mRNA is not bound by ribosomes, the linker probe hybridizes weakly to extensions on the ribosome probes and the mRNA interaction probes and can be washed out of cells. (B) NIH 3T3 fibroblasts hybridized with either ribosome probes, mRNA interaction probes to β-actin, or both ribosome and β-actin mRNA interaction probes (top, green, Alexa 546 fluorescence). Cells are simultaneously hybridized with β-actin transcript probes (middle, red, Alexa 488 fluorescence). Nuclei are stained with DAPI (blue). Merge of ribosome-mRNA interaction signals and transcript signals (bottom). Scale bar = 10 μm. (C) Zoom of single mRNA molecules. Red spot: mRNA transcript without ribosome interaction. Yellow spots: mRNA transcripts with ribosome interaction. Scale bar = 1 μm. (D) Fraction of β-actin transcript spots colocalized with ribosome-mRNA interaction spots. Error bars, standard deviation. Data represents two independent experiments, n = 10 or 11 cells per experiment.

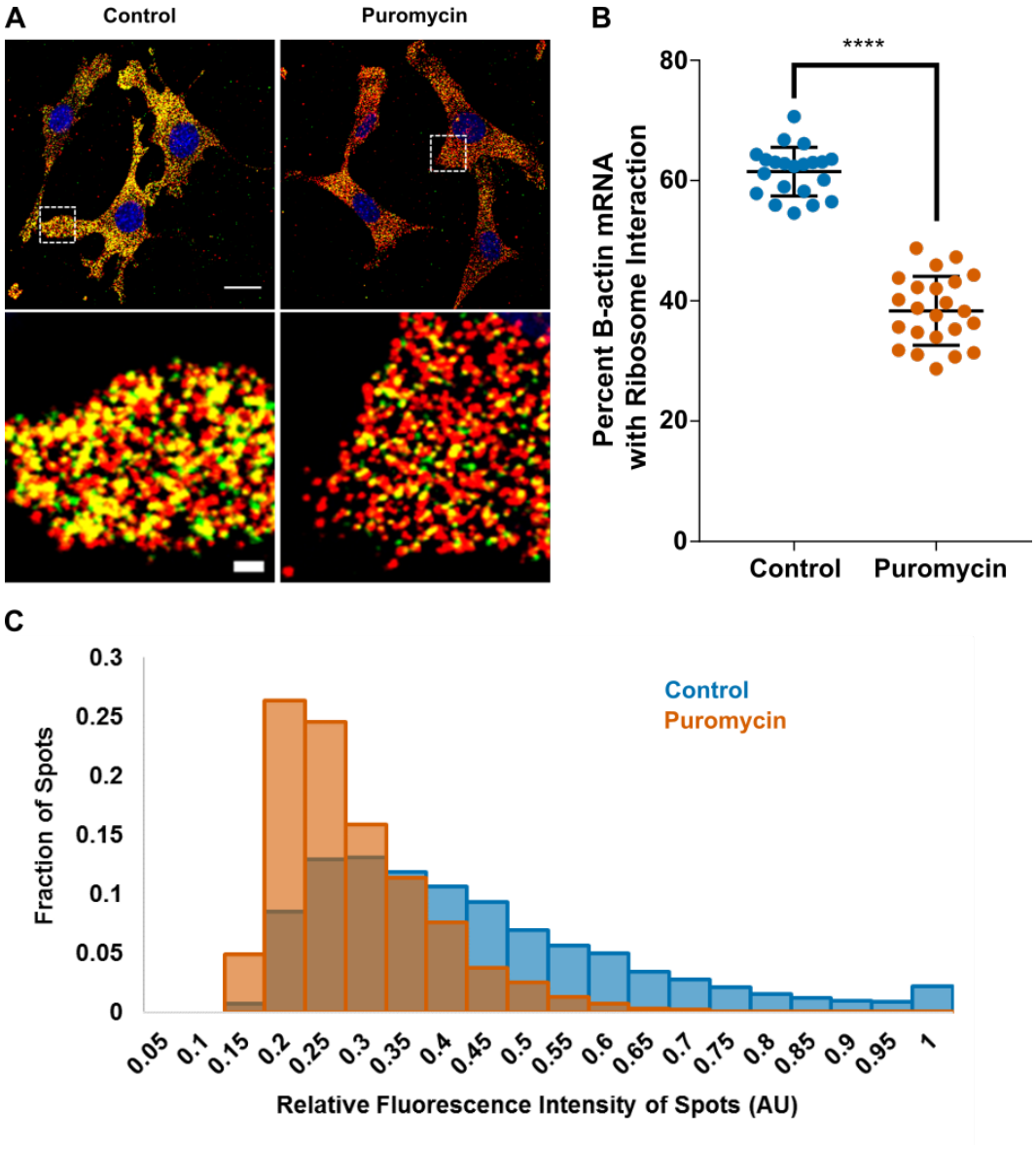
A
Control
Puromycin
B
****
Percent B-actin mRNA with Ribosome Interaction
80
60
40
20
0
Control
Puromycin
C
Fraction of Spots
0.3
0.25
0.2
0.15
0.1
0.05
0
Control
Puromycin
0.05
0.1
0.15
0.2
0.25
0.3
0.35
0.4
0.45
0.5
0.55
0.6
0.65
0.7
0.75
0.8
0.85
0.9
0.95
1
Relative Fluorescence Intensity of Spots (AU)

Figure 2.2 (*previous page*): The translation inhibitor puromycin causes a significant decrease in ribosome-mRNA interaction as detected by FLARIM. (A) Ribosome-mRNA interaction images for β-actin in NIH 3T3 cells that were either untreated (left) or treated (right) with puromycin at 200 μg/mL for 1 h. In the puromycin sample, there is a noticeable decrease in detectable colocalization (yellow) between β-actin mRNA transcript signals (red, Alexa 488 fluorescence) and ribosome-mRNA interaction signals (green, Alexa 546 fluorescence). Top, scale bar = 20 μm. Bottom, scale bar = 2 μm. (B) Fraction of β-actin mRNA transcript spots per cell colocalized with a ribosome-mRNA interaction spot, with and without puromycin treatment. Dots represent single cells. Data represent two independent experiments. n = 7 – 16 cells per condition per experiment. Error bars, standard deviation. ****$P<0.0001$, Student's t-test. (C) Distribution of fluorescence intensities of ribosome-mRNA interaction spots for β-actin, with and without puromycin treatment. Representative data from one experiment. Control, n = 10 cells and 11,314 spots; puromycin, n = 7 cells and 5,343 spots.

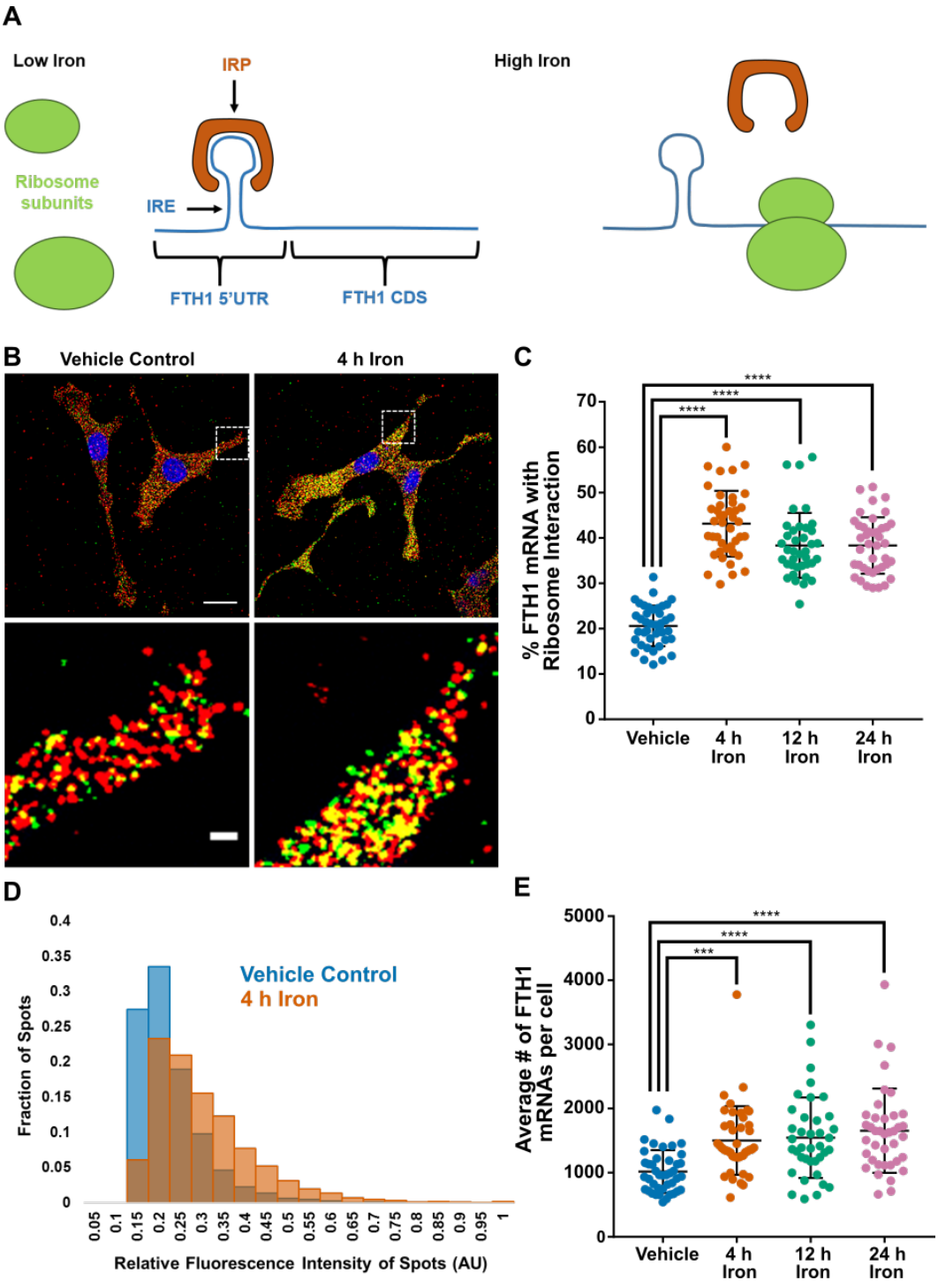
A
Low Iron
IRP
Ribosome subunits
IRE
FTH1 5'UTR
FTH1 CDS
High Iron
B
Vehicle Control
4 h Iron
C
% FTH1 mRNA with Ribosome Interaction
Vehicle
4 h Iron
12 h Iron
24 h Iron
D
Fraction of Spots
Vehicle Control
4 h Iron
Relative Fluorescence Intensity of Spots (AU)
E
Average # of FTH1 mRNAs per cell
Vehicle
4 h Iron
12 h Iron
24 h Iron

Figure 2.3 (*previous page*): Changes in FTH1 expression in response to added iron are detected by FLARIM. (A) Schematic of translational regulation of FTH1 mRNA by iron. (B) Images illustrating increase in ribosome-mRNA interaction for FTH1 after iron treatment for 4 h (right) compared to a vehicle control (left). In the iron-treated sample, there is a noticeable increase in detectable colocalization (yellow) between FTH1 mRNA transcript signals (red, Alexa 488 fluorescence) and ribosome-mRNA interaction signals (green, Alexa 546 fluorescence). Representative results from three independent experiments are shown. Scale bar = 20 μm. (C) Fraction of FTH1 mRNA transcript spots per cell colocalized with a ribosome-mRNA interaction spot, with and without iron treatment over time. Dots represent single cells. Data represent three independent experiments. n = 10-17 cells per condition per experiment. Error bars, standard deviation. ****P<0.0001 (one-way ANOVA with Dunnett's test). (D) Distribution of fluorescence intensities of ribosome-mRNA interaction spots for FTH1 in cells treated with iron for 4 h compared to a vehicle control. Representative results from one experiment. Vehicle, n = 17 cells and 3,503 spots; 4 h, n = 15 cells and 9,106 spots. (E) Changes in FTH1 mRNA level per cell, with and without iron treatment for 4 h. Error bars, standard deviation. ***P<0.0002, ****P<0.0001 (one-way ANOVA with Dunnett's test).

2.7 Supplemental Data and Figures

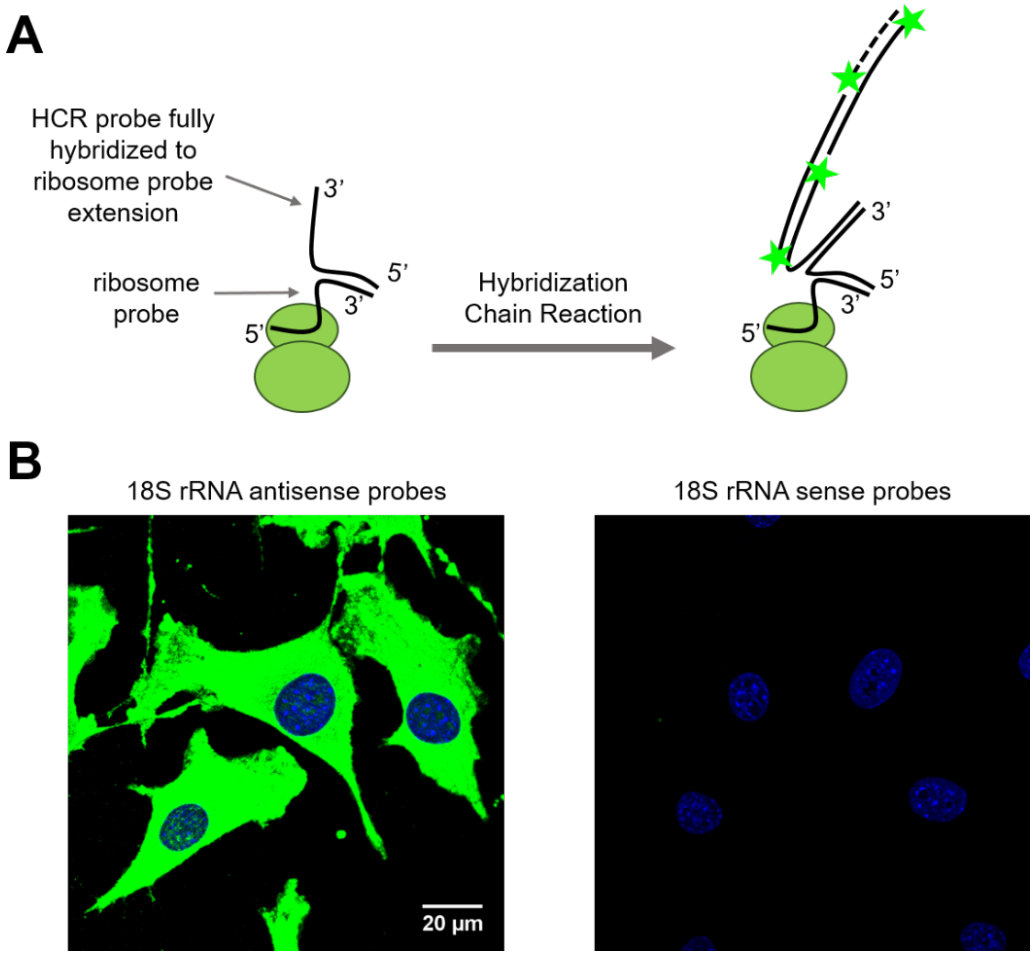

Figure 2.S1: rRNA FISH in NIH 3T3 fibroblasts. (A) Schematic of experimental design to measure fluorescence from ribosome probes. Multiple ribosomes probes are hybridized to the 18S rRNA, but for illustration purposes, only a single probe is shown. (B) Fluorescence from antisense or sense probes for 18S rRNA. Green = ribosome signal, Blue = DAPI. Bright fluorescence signal is detected throughout cells with antisense probes. No signal is detected with sense probes.

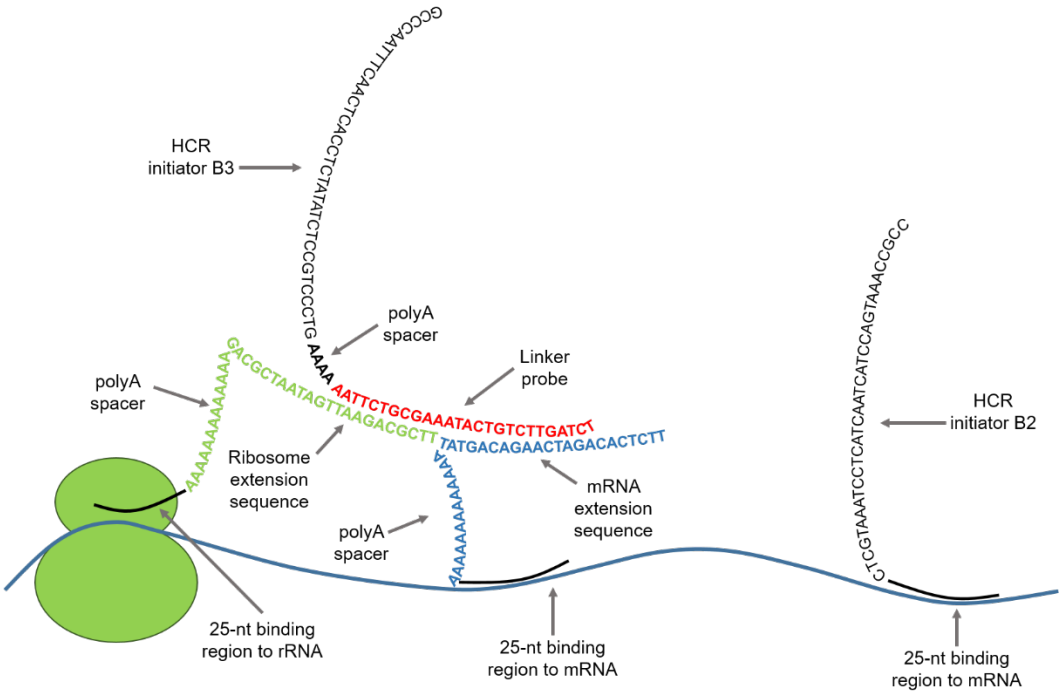

Figure 2.S2: Schematic showing shared nucleotide sequences of ribosome probes and mRNA probes, as well as the sequence and binding location of the linker probe.

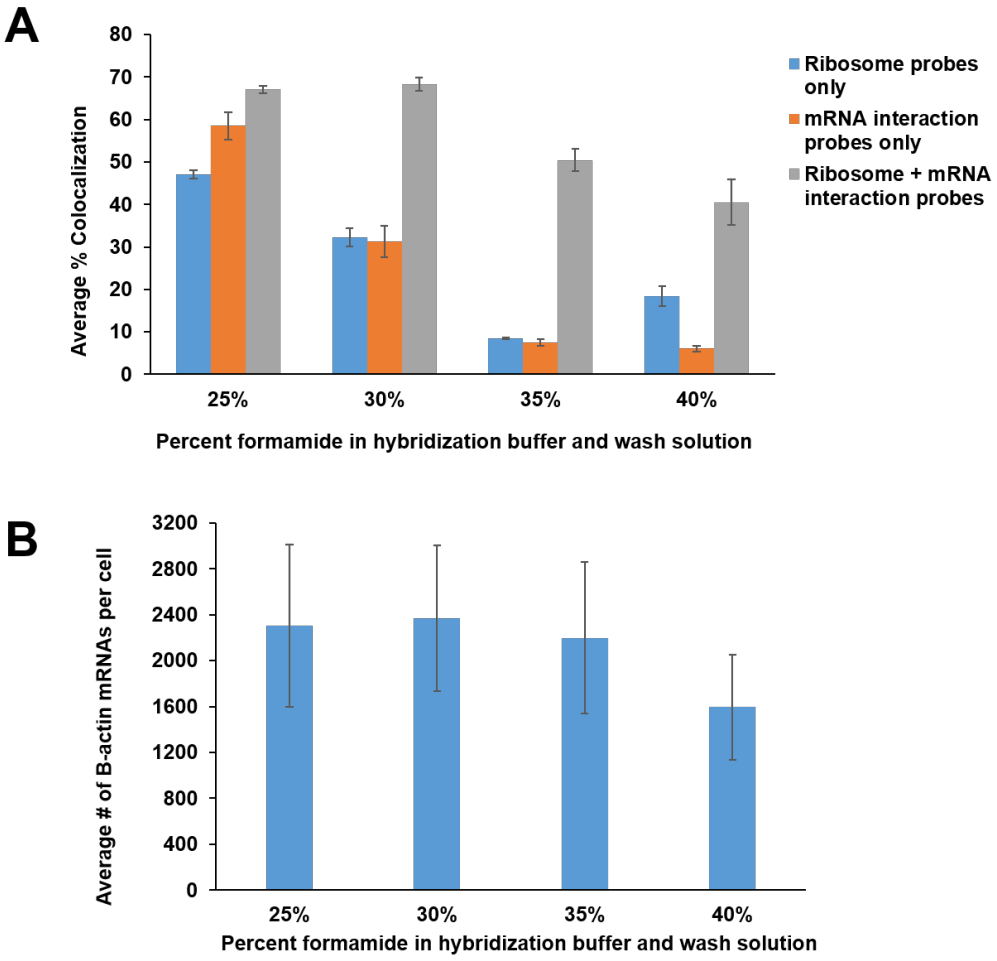

Figure 2.S3: Effect of formamide concentration in the linker hybridization buffer and wash solution on FLARIM results. Effect on (A) colocalization of β-actin mRNA transcript signals to background signal relative to ribosome-mRNA interaction signal and (B) hybridization of the β-actin mRNA transcript probes. In solutions with 25% and 30% formamide, the colocalization of β-actin transcript signals to ribosome or mRNA interaction probes alone may contribute significantly to the colocalization measured with both probes added. The buffer and wash solution with 40% formamide compromises hybridization of mRNA transcript probes, resulting in a significantly lower measure of mRNA transcripts per cell. Therefore, we chose 35% formamide for all experiments in this study. Error bars, standard deviation. For (A) and (B), n = 3-9 cells or 20-27 cells per measurement, respectively.

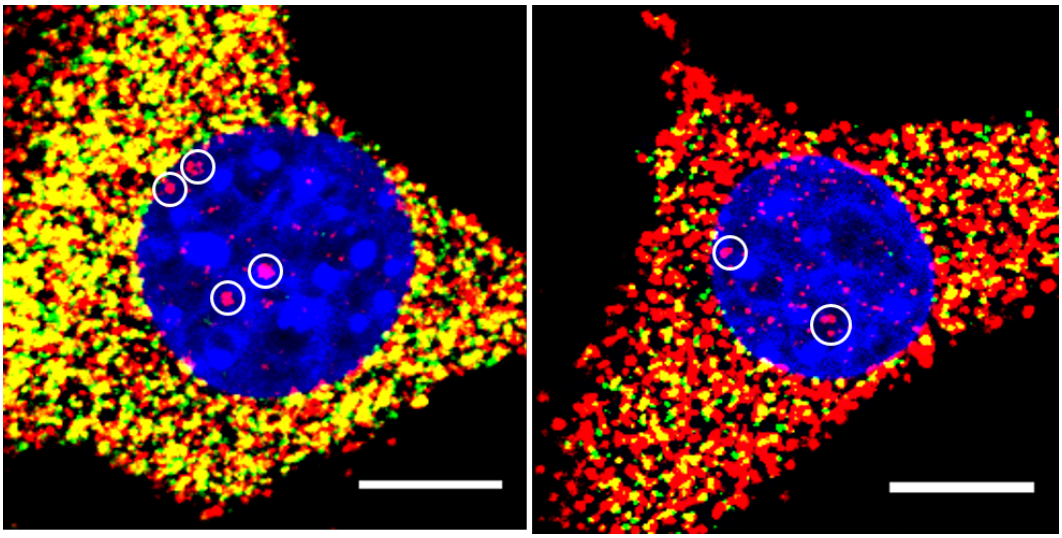

Figure 2.S4: Interaction of β-actin and FTH1 with ribosomes in cell nuclei. Confocal images of ribosome-mRNA interactions for β-actin (left) and FTH1 (right). Images show merged signals from Alexa 488 and Alexa 546 channels. Red = Alexa 488 fluorescence from mRNA transcript probes. Green = Alexa 546 fluorescence from mRNA interaction probes. Yellow = colocalization of red and green indicating an mRNA with bound ribosomes. Circled red spots in the nucleus illustrate lack of ribosome interaction with these transcripts. Scale bar = 10 μm. The fraction of β-actin transcript spots colocalized with ribosomes in the nucleus is 0.12 ± 0.12 (n = 10 cells). The fraction of FTH1 transcript probes colocalized with ribosomes in the nucleus is 0.12 ± 0.08 (n = 15 cells).

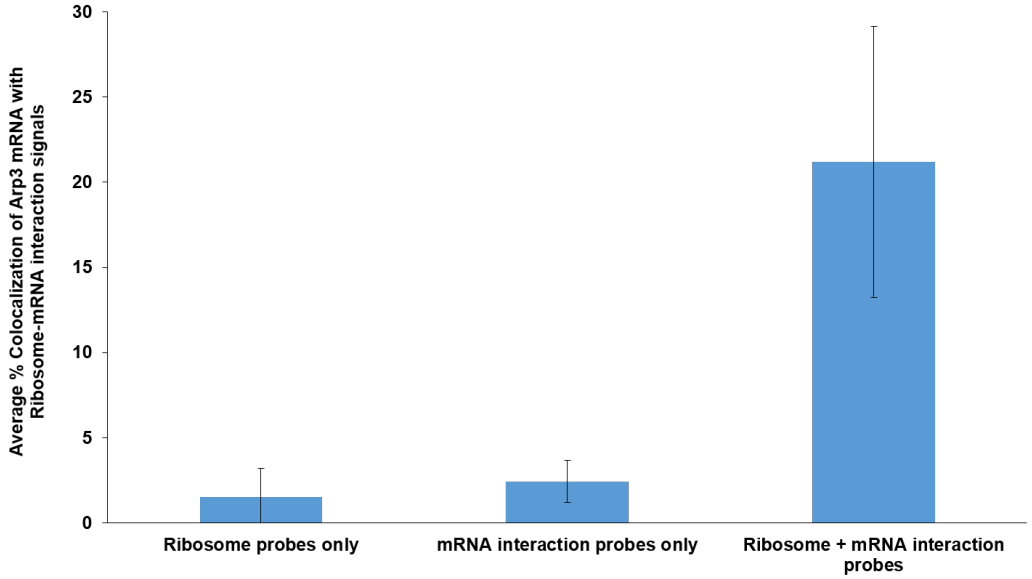

Figure 2.S5: Fraction of Arp3 transcript spots colocalizing with ribosome-mRNA interaction spots, when different probe sets are added: ribosome probes only, Arp3 mRNA interaction probes only, or the combination of ribosome and Arp3 mRNA interaction probes. Error bars, standard deviation. Data represents three independent experiments, n = 20 – 31 cells per measurement.

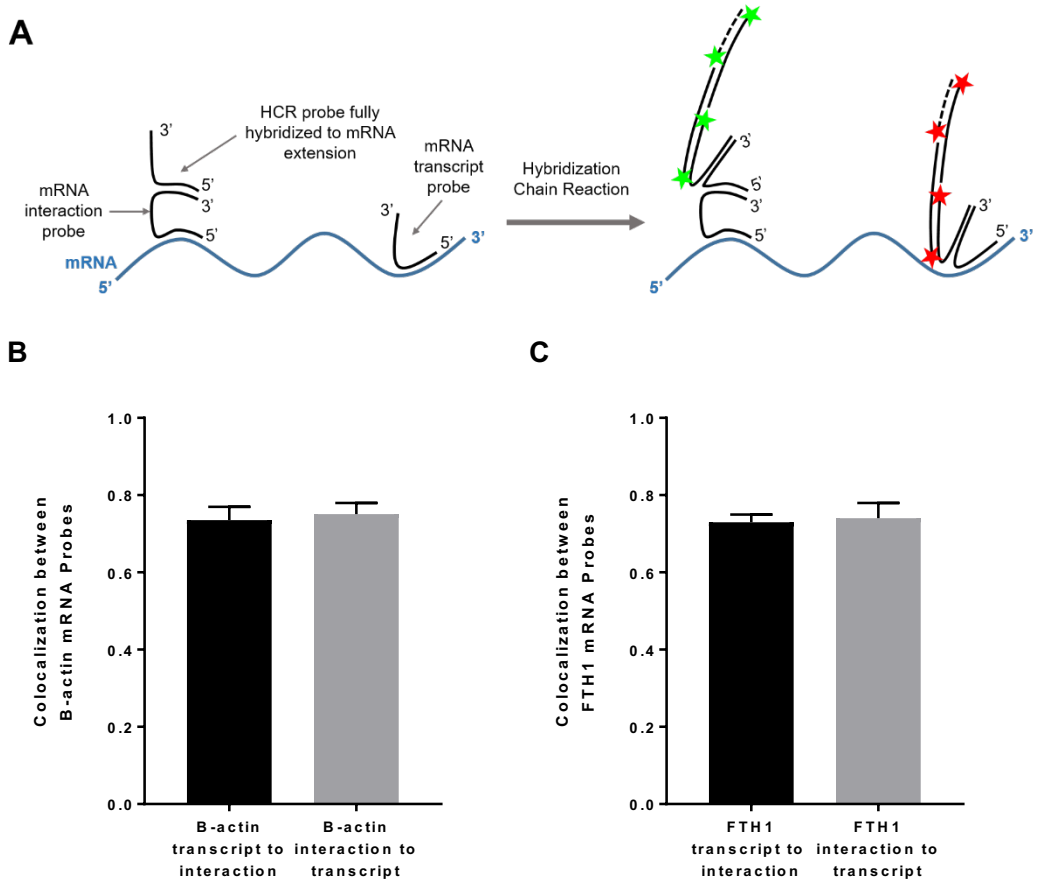

Figure 2.S6: Colocalization between transcript probes and interaction probes for β-actin and FTH1. (A) Schematic of experimental design to test extent of colocalization between mRNA interaction and transcript probes. Multiple interaction and transcript probes are hybridized to a single mRNA, but for illustration purposes, only a single probe per type is shown. (B) Average colocalization between β-actin mRNA probes in the cytoplasm. The fraction of β-actin transcript probes colocalized with interaction probes is 0.74 ± 0.03. The fraction of interaction probes colocalized with transcript probes is 0.75 ± 0.03. Data represent two independent experiments, n = 8 cells. (C) Average colocalization between FTH1 mRNA probes in the cytoplasm. The fraction of FTH1 transcript probes colocalized with interaction probes is 0.73 ± 0.02. The fraction of interaction probes colocalized with transcript probes is 0.74 ± 0.04. Data represent three independent experiments, n = 20 cells.

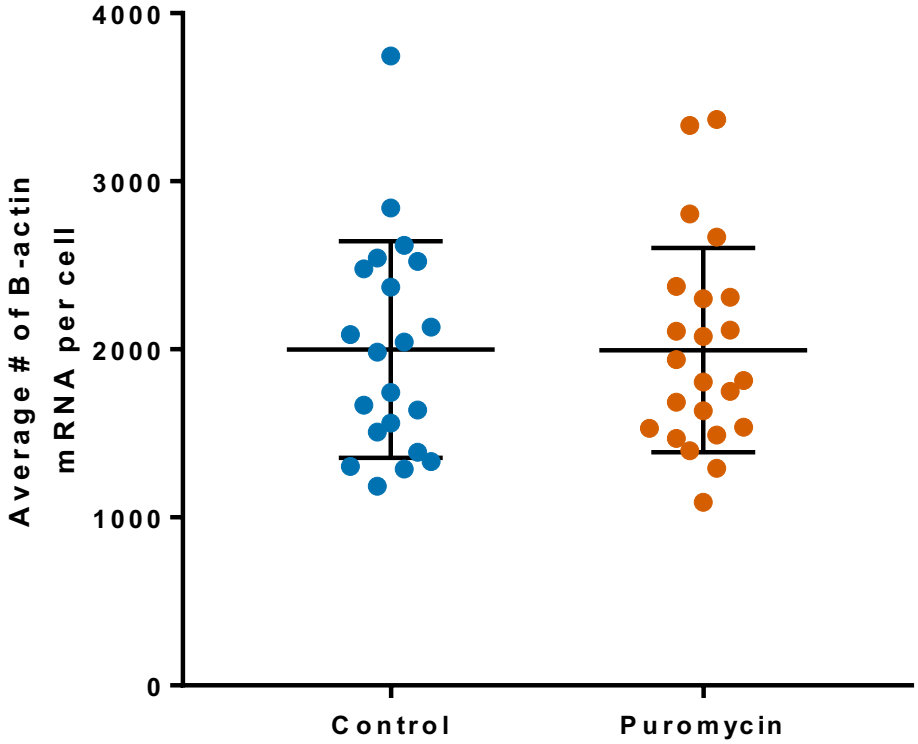

Figure 2.S7: Levels of β-actin mRNA in control and puromycin-treated NIH 3T3 fibroblasts. The average numbers (± standard deviation) of β-actin mRNAs per cell are 1999 ± 645 (n = 21 cells) and 1995 ± 608 (n = 23 cells) for control and puromycin-treated cells, respectively. Differences in the values are not statistically significant, P = 0.9843.

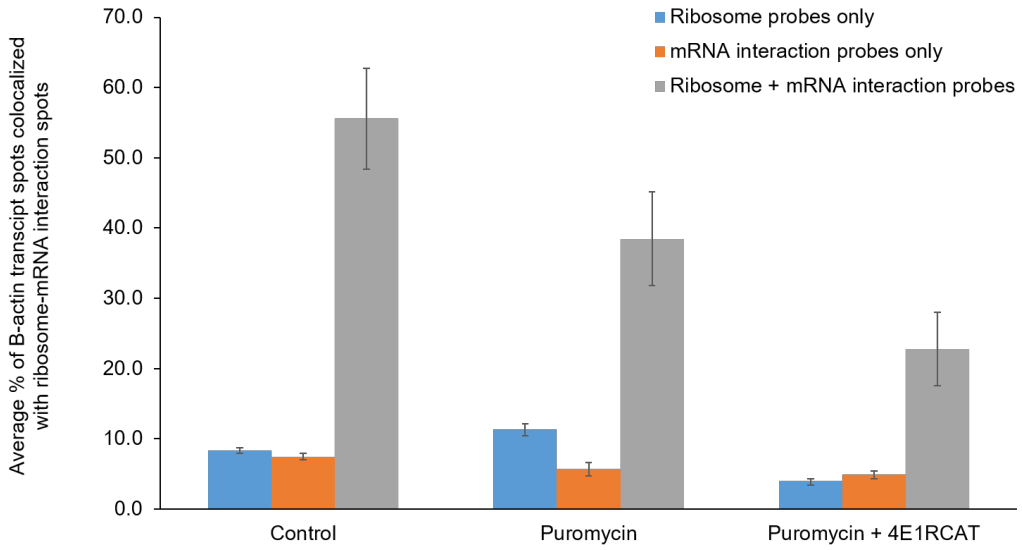

Figure 2.S8: Effect of puromycin in combination with 4E1RCAT on interaction of β-actin mRNA with ribosomes. Fraction of β-actin mRNA transcript spots per cell colocalized with a ribosome-mRNA interaction spot after no treatment (Control), treatment with 200 ug/mL of puromycin for 1 h, or treatment 200 μg/mL of puromycin and 5 μM 4E1RCat for 1 h. n = 3-14 cells per measurement. Error bars, standard deviation. We thank a reviewer for suggesting this experiment.

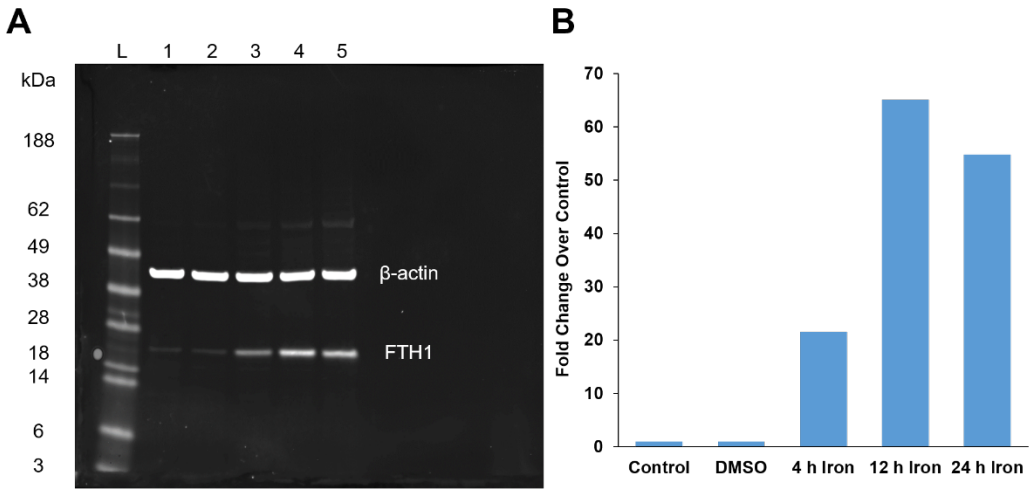

Figure 2.S9: (A) Western blot and (B) quantification of increased FTH1 protein levels in NIH 3T3 cells treated with iron in the form of hemin at 50 μM for 4, 12, and 24 h. Lysates were first blotted against primary antibodies for FTH1 and β-actin and then blotted against a goat anti-rabbit IgG secondary antibody coupled to Alexa 488. β-actin was used as a loading control. L = ladder, 1 = No treatment, 2 = 0.2% DMSO for 24 h (vehicle), 3 = 4 h hemin, 4 = 12 h hemin, 5 = 24 h hemin. We used ImageQuant TL software to quantify the fold change in FTH1 protein level per treatment condition compared to the control. We first performed a background subtraction of the Western blot with the rolling ball method to remove the baseline intensity. We then measured the integrated intensity of each band and determined the ratio of the FTH1 band intensity to the β-actin band intensity per lane. The fold change for each treatment condition was calculated by dividing its band intensity ratio for by the ratio of the control lane.

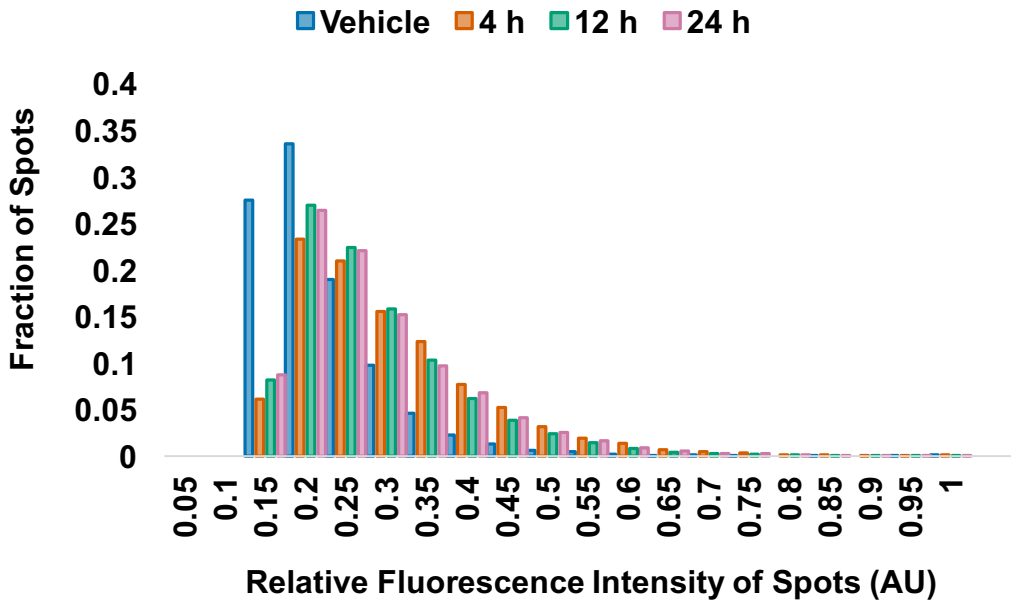

Figure 2.S10: Distribution of fluorescence intensities of ribosome-mRNA interaction spots for FTH1 in cells treated with iron for 4 h, 12 h, or 24 h compared to a vehicle control. Representative results from one experiment. Vehicle, n = 10 cells and 2770 spots; 4 h, n = 16 cells and 13360 spots; 12 h, n = 16 cells and 11392 spots; 24 h, n = 15 cells and 11890 spots.

2.8 Supplemental Tables

Table 2.S1: Sequences of all oligonucleotide probes used in Chapter 2. Provided as a separate Excel file.

Table 2.S2: Probe sequences for human 18S rRNA. Provided as a separate Excel file.

Table 2.S3: Fraction (average ± standard deviation) of putative β-actin transcripts (Alexa 488 spots) in the cytoplasm colocalized with Alexa 546 spots, which may correspond to linker probes or dye-labeled HCR hairpins, when only β-actin interaction probes, only ribosomes probes, or neither are added. Data represent two independent experiments. n = 4-6 cells per measurement per experiment.

	Ribosome probes only	mRNA interaction probes only	Neither ribosome nor mRNA interaction probes (Linker + HCR background)
Control	0.08 ± 0.01	0.07 ± 0.02	0.007 ± 0.003
Puromycin	0.09 ± 0.03	0.09 ± 0.03	0.004 ± 0.002

Table 2.S4: Fraction (average ± standard deviation) of putative FTH1 transcripts (Alexa 488 spots) in the cytoplasm colocalized with Alexa 546 spots, which may correspond to linker probes or dye-labeled HCR hairpins, when FTH1 interaction probes, ribosomes probes, or both are omitted. Data represent three independent experiments. n = 5-9 cells per measurement per experiment.

	Ribosome probes only	mRNA interaction probes only	Neither ribosome nor mRNA interaction probes (Linker + HCR background)
Vehicle	0.06 ± 0.02	0.02 ± 0.02	0.006 ± 0.004
4h	0.06 ± 0.02	0.04 ± 0.01	0.005 ± 0.003
12h	0.05 ± 0.02	0.04 ± 0.02	0.005 ± 0.003
24h	0.07 ± 0.01	0.04 ± 0.01	0.005 ± 0.002

Table 2.S5: Fraction of ribosome-mRNA interaction spots colocalized with β-actin transcript spots with or without puromycin treatment. Data represent two independent experiments. n = 4-6 cells per measurement per experiment.

	Fraction of spots
Control	0.68 ± 0.04
Puromycin	0.68 ± 0.03

Table 2.S6: Fraction of ribosome-mRNA interaction spots colocalized with FTH1 transcript spots after different treatments with iron. Data represent three independent experiments. n = 5-9 cells per measurement per experiment.

	Fraction of spots
Vehicle	0.54 ± 0.05
4h	0.57 ± 0.04
12h	0.55 ± 0.05
24h	0.58 ± 0.03

2.9 Methods

Dulbecco's Modified Eagle Medium (DMEM) (#12491015), Fetal Bovine Serum (FBS) (#10438026), Penicillin-Streptomycin (5,000 U/mL) (#15070063), Trypsin-EDTA (0.05%) (#25300054), RIPA buffer (#89900), and Human Plasma Fibronectin (#33016015) were purchased from ThermoFisher (Tustin, CA). SecureSeal hybridization chambers (8 well, 7mm x 7mm x 0.8mm, SKU 621503) were purchased from Grace BioLabs (Bend, OR), and 22mm x 50mm No. 1 glass coverslips were purchased from VWR (Brisbane, CA). All DNA oligonucleotide probes were designed using Stellaris Probe Designer version 4.2 (LGC Biosearch Technologies) and purchased from Integrated DNA Technologies (San Diego, CA). HCR hairpins were purchased pre-coupled to fluorophores from Molecular Instruments (Pasadena, CA). Formamide (SKU F9037), dextran sulfate (SKU D8906), puromycin (SKU P8833), hemin (SKU 51280), Benzonase Nuclease (SKU E1014) and cOmplete Protease Inhibitor Cocktail (SKU 4693116001) were purchased from Sigma-Aldrich (St. Louis, MO). Primary antibodies for FTH1 (ab183781) and ACTB (ab8227) were purchased from Abcam (Burlingame, CA). A goat anti-rabbit IgG secondary antibody coupled to Alexa 488 (A-11034) was purchased from Life Technologies (Carlsbad, CA).

Images were acquired on a Zeiss LSM 800 laser scanning confocal microscope operated by the Biological Imaging Facility of the Beckman Institute at Caltech. Imaging data were analyzed with the FISH-quant program written by Florian Mueller, the Cell Profiler program developed by the Broad Institute Imaging Platform, and the XPIWIT software tool developed by Johannes Stegmaier and the Center for Advanced Methods in Biological Image Analysis at the Beckman Institute (CAMBIA).

Cell Culture. NIH 3T3 fibroblasts were grown in DMEM supplemented with 10% fetal bovine serum (FBS), 50 units/mL penicillin, and 50 μg/mL streptomycin at 37˚C in 5% CO_2. Cells were passaged 2-3 times per week. In preparation for each imaging experiment, cells were trypsinized and transferred to glass coverslips pre-coated with

10 μg/mL human plasma fibronectin in 1X PBS, then grown on the coverslips overnight.

For puromycin and hemin treatments, cells were grown on coverslips overnight and then the appropriate reagent was added directly to the cell culture medium. Cells were incubated with the reagents at 37˚C and 5% CO_2. Puromycin was added at a final concentration of 200 μg/mL (from a stock 50-mg/mL solution in water) and left for 1 h. Hemin was added at a final concentration of 25 μM (from a 50-mM stock solution in DMSO) and left for 4 h, 12 h, or 24 h. A vehicle control sample was incubated with 0.2% DMSO for 24 h. Hemin stocks were prepared fresh before each experiment.

***In Situ* Hybridization and Hybridization Chain Reaction (HCR)**. Cells were fixed with 4% formaldehyde in 1X PBS for 30 min at room temperature (25°C). The reaction was quenched with 0.1 M glycine in 1X PBS for 5 min and then cells were washed once with 1X PBS. Fixed cells were permeabilized with 0.1% SDS in 1X PBS for 10 min with gentle rocking. Cells were washed once with 0.1% Triton in 1X PBS, then twice with 1X PBS. Cells were stored in 70% ethanol at 4˚C for at least 2 h and up to 3 days before hybridization.

For hybridization, coverslips were removed from ethanol and air dried. Secure-Seal hybridization chambers were attached to each coverslip. Cells were incubated overnight at 37˚C in a humid chamber with 1-2 nM/oligo of probes for ribosomes and mRNA in a hybridization buffer of 10% formamide and 10% dextran sulfate in 2X SSC.

The next day, the probe solutions were removed, and cells were washed three times with a solution of 35% formamide and 0.1% Triton in 2X SSC, then three times with 2X SSC, to remove excess probes not bound to RNA. Cells were then incubated for 30 min at 40˚C with a pre-heated solution of 10 nM linker probe in a hybridization buffer consisting of 35% formamide and 10% dextran sulfate in 2X SSC (“linker hybridization buffer”). After incubation, cells were washed three times with 0.1%

Triton in 2X SSC and twice with 2X SSC, then were left to cool for 15-20 min at room temperature. Cells were finally washed three times with 35% formamide and 0.1% Triton in 2X SSC and three times with 2X SSC to remove any unbound or partially-hybridized linker probes.

For HCR, the basic protocol of Choi and coworkers was followed with modifications[17]. Fluorescently labeled HCR hairpins were first snap-cooled (heated to 95˚C for 90 sec, then allowed to cool at room temperature for 30 min). The cells were then incubated for 1 h at room temperature (25˚C) with 85 nM hairpins in a hybridization buffer of 10% dextran sulfate in 2X SSC. Following HCR, the cells were washed twice with 0.1% Triton in 2X SSC, incubated with 1 μg/mL DAPI for 1 min, washed twice with 2X SSC, and then kept in 2X SSC for imaging.

Western Blot. Cells were left untreated, incubated with 50-μM hemin (from a 50-mM stock solution in DMSO) for 4 h, 12h, or 24h, or incubated with 0.2% DMSO for 24 h as a vehicle control. Cells were then washed with cold PBS and lysed in RIPA buffer supplemented with one cOmplete protease inhibitor tablet per 10 mL of buffer for 30 min on ice with gentle rocking. Lysates were collected using a cell scraper and were treated with 1 μL of Benzonase Nuclease per 500 μL of lysate for 10 min at 37˚C. Lysates were heated in a loading buffer containing 50 mM Tris-HCl (pH 6.8), 2% SDS, 0.1% bromophenol blue, 10% glycerol, and 5% BME at 95˚C for 10 min and immediately loaded onto a pre-cast SDS PAGE gel. Each lane was loaded with 15 μg of protein. After electrophoretic separation, proteins were transferred to a nitrocellulose membrane, which was blocked with 5% nonfat dry milk (NFDM) in PBS and 0.1% Tween-20 (PBST) for 1 h. The membrane was then incubated with a 1/1000 dilution each of the FTH1 antibody and ACTB loading control in 5% NFDM in PBST overnight at 4˚C with gentle rocking. The next day, the membrane was washed three times with PBST for 10 min each with gentle rocking. The membrane was then incubated with an Alexa Fluor 488-conjugated secondary antibody at 1/10,000 dilution in 5% NFDM in PBST at room temperature for 1 h. The membrane

was washed three times with PBST for 5 min each and imaged with a Typhoon Trio Imager.

Fluorescence Imaging. All images were collected with a Zeiss LSM 800 laser scanning confocal microscope, using a 63X, NA 1.4 Plan-Apochromat objective. Resolution was set to 1024 x 1024 with a digital zoom of 0.7X and line averaging of 2. Excitation laser sources and emission ranges were 405 nm/400-510 nm (DAPI, shown as blue), 488 nm/510-560 nm (Alexa 488, shown as red), and 561 nm/560-700 nm (Alexa 546, shown as green). Each image was collected as a 3D stack of 15-30 images with a spacing of 0.4 μm in the z-direction between slices.

Image Analysis. Images were analyzed using the MATLAB-based program FISH-quant[59]. Outlines of cells and nuclei were drawn manually in FISH-quant or automatically using Cell Profiler[60]. A 3D dual-Gaussian filter was used in FISH-quant for background subtraction. Spots corresponding to ribosome-mRNA interactions or mRNA transcripts were identified by fitting with a 3D Gaussian function. The intensity and the width of the 3D Gaussian were thresholded to exclude autofluorescence and non-specific signals. Ribosome-mRNA interaction spots and mRNA transcript spots were identified independently and then analyzed for colocalization. The distance threshold for colocalization was set at 420 nm, which is equal to 3 pixels in all of our images. Raw intensity values were used for measurements of fluorescence intensity. For measuring colocalization of nuclear transcripts, a custom processing pipeline was implemented in the XPIWIT software tool to create a 3D mask based on DAPI fluorescence for each image[61]. The pipeline consisted of a median filter for noise reduction, a binarization of the image using Otsu's method and a morphological closing to remove holes in the mask. The final 3D mask was multiplied with the raw images, and thus only the spots within the 3D mask were kept for analysis. Any remaining spots on the edges of the nuclear mask were removed manually in FISH-quant before colocalization analysis.

2.10 References

(1) Gygi, S. P.; Rochon, Y.; Franza, B. R.; Aebersold, R. Correlation between Protein and mRNA Abundance in Yeast. *Mol. Cell. Biol.* **1999**, *19*, 1720–1730 DOI: 10.1128/MCB.19.3.1720.

(2) Ideker, T.; Thorsson, V.; Ranish, J. A.; Christmas, R.; Buhler, J.; Eng, J. K.; Bumgarner, R.; Goodlett, D. R.; Aebersold, R.; Hood, L. Integrated Genomic and Proteomic Analyses of a Systematically Perturbed Metabolic Network. *Science* **2001**, *292*, 929–934 DOI: 10.1126/science.292.5518.929.

(3) Ingolia, N. T.; Ghaemmaghami, S.; Newman, J. R. S.; Weissman, J. S. Genome-Wide Analysis in Vivo of Translation with Nucleotide Resolution Using Ribosome Profiling. *Science* **2009**, *324*, 218–223 DOI: 10.1126/science.1168978.

(4) Taniguchi, Y.; Choi, P. J.; Li, G.; Chen, H.; Babu, M.; Hearn, J.; Emili, A.; Xie, X. S. Quantifying E. Coli Proteome and Transcriptome with Single-Molecule Sensitivity in Single Cells. *Science* **2010**, *329*, 533–538 DOI: 10.1126/science.1188308.

(5) Schwanhäusser, B.; Busse, D.; Li, N.; Dittmar, G.; Schuchhardt, J.; Wolf, J.; Chen, W.; Selbach, M. Global Quantification of Mammalian Gene Expression Control. *Nature* **2011**, *473*, 337–342 DOI: 10.1038/nature10098.

(6) Shestakova, E. A.; Singer, R. H.; Condeelis, J. The Physiological Significance of β-Actin mRNA Localization in Determining Cell Polarity and Directional Motility. *Proc. Natl. Acad. Sci. U. S. A.* **2001**, *98*, 7045–7050 DOI: 10.1073/pnas.121146098.

(7) Hüttelmaier, S.; Zenklusen, D.; Lederer, M.; Dictenberg, J.; Lorenz, M.; Meng, X.; Bassell, G. J.; Condeelis, J.; Singer, R. H. Spatial Regulation of β-Actin Translation by Src-Dependent Phosphorylation of ZBP1. *Nature* **2005**, *438*, 512–515 DOI: 10.1038/nature04115.

(8) Curtis, D.; Lehmann, R.; Zamore, P. D. Translational Regulation in Development. *Cell* **1995**, *81* (2), 171–178 DOI: 10.1016/0092-8674(95)90325-9.

(9) Holcik, M.; Sonenberg, N. Translational Control in Stress and Apoptosis. *Nat. Rev. Mol. Cell Biol.* **2005**, *6*, 318–327 DOI: 10.1038/nrm1618.

(10) Costa-mattioli, M.; Sossin, W. S.; Klann, E.; Sonenberg, N. Translational Control of Long-Lasting Synaptic Plasticity and Memory. *Neuron* **2009**, *61*, 10–26 DOI: 10.1016/j.neuron.2008.10.055.

(11) Mortazavi, A.; Williams, B. A.; McCue, K.; Schaeffer, L.; Wold, B. Mapping and Quantifying Mammalian Transcriptomes by RNA-Seq. *Nat. Methods* **2008**, *5*, 621–628 DOI: 10.1038/nmeth.1226.

(12) Jan, C. H.; Williams, C. C.; Weissman, J. S. Principles of ER Cotranslational Translocation Revealed by Proximity-Specific Ribosome Profiling. *Science* **2014**, *346*, 1–8 DOI: 10.1126/science.1257521.

(13) Williams, C. C.; Jan, C. H.; Weissman, J. S. Targeting and Plasticity of Mitochondrial Proteins Revealed by Proximity-Specific Ribosome Profiling. *Science* **2014**, *346*, 748–751 DOI: 10.1126/science.1257522.

(14) Gandin, V.; Sikström, K.; Alain, T.; Morita, M.; McLaughlan, S.; Larsson, O.; Topisirovic, I. Polysome Fractionation and Analysis of Mammalian Translatomes on a Genome-Wide Scale. *J. Vis. Exp.* **2014**, *87*, 1–10 DOI: 10.3791/51455.

(15) Tang, F.; Barbacioru, C.; Wang, Y.; Nordman, E.; Lee, C.; Xu, N.; Wang, X.; Bodeau, J.; Tuch, B. B.; Siddiqui, A.; Lao, K.; Surani, M. A. mRNA-Seq Whole-Transcriptome Analysis of a Single Cell. *Nat. Methods* **2009**, *6*, 377–382 DOI: 10.1038/nmeth.1315.

(16) Rodriguez, A. J.; Shenoy, S. M.; Singer, R. H.; Condeelis, J. Visualization of mRNA Translation in Living Cells. *J. Cell Biol.* **2006**, *175*, 67–76 DOI: 10.1083/jcb.200512137.

(17) Choi, H. M. T.; Beck, V. A.; Pierce, N. A. Next-Generation in Situ Hybridization Chain Reaction : Higher Gain , Lower Cost , Greater Durability. *ACS Nano* **2014**, *8*, 4284–4294 DOI: 10.1021/nn405717p C2014.

(18) Wang, F.; Flanagan, J.; Su, N.; Wang, L. C.; Bui, S.; Nielson, A.; Wu, X.; Vo, H. T.; Ma, X. J.; Luo, Y. RNAscope: A Novel in Situ RNA Analysis Platform

for Formalin-Fixed, Paraffin-Embedded Tissues. *J. Mol. Diagnostics* **2012**, *14*, 22–29 DOI: 10.1016/j.jmoldx.2011.08.002.

(19) Shah, S.; Lubeck, E.; Schwarzkopf, M.; He, T.; Greenbaum, A.; Sohn, C. H.; Lignell, A.; Choi, H. M. T.; Gradinaru, V.; Pierce, N. A.; Cai, L. Single-Molecule RNA Detection at Depth via Hybridization Chain Reaction and Tissue Hydrogel Embedding and Clearing. *Development* **2016**, *143*, 2862–2867 DOI: 10.1242/dev.138560.

(20) Ong, S. Stable Isotope Labeling by Amino Acids in Cell Culture, SILAC, as a Simple and Accurate Approach to Expression Proteomics. *Mol. Cell. Proteomics* **2002**, *1*, 376–386 DOI: 10.1074/mcp.M200025-MCP200.

(21) Dieterich, D. C.; Link, A. J.; Graumann, J.; Tirrell, D. A.; Schuman, E. M. Selective Identification of Newly Synthesized Proteins in Mammalian Cells Using Bioorthogonal Noncanonical Amino Acid Tagging (BONCAT). *Proc. Natl. Acad. Sci. U. S. A.* **2006**, *103*, 9482–9487 DOI: 10.1073/pnas.0601637103.

(22) Dieterich, D. C.; Hodas, J. J. L.; Gouzer, G.; Shadrin, I. Y.; Ngo, J. T.; Triller, A.; Tirrell, D. A.; Schuman, E. M. In Situ Visualization and Dynamics of Newly Synthesized Proteins in Rat Hippocampal Neurons. *Nat. Neurosci.* **2010**, *13*, 897–905 DOI: 10.1038/nn.2580.

(23) Starck, S. R.; Green, H. M.; Alberola-Ila, J.; Roberts, R. W. A General Approach to Detect Protein Expression In Vivo Using Fluorescent Puromycin Conjugates. *Chem. Biol.* **2004**, *11*, 999–1008 DOI: 10.1016/j.chembiol .2004.05.011.

(24) David, A.; Dolan, B. P.; Hickman, H. D.; Knowlton, J. J.; Clavarino, G.; Pierre, P.; Bennink, J. R.; Yewdell, J. W. Nuclear Translation Visualized by Ribosome-Bound Nascent Chain Puromycylation. *J. Cell Biol.* **2012**, *197*, 45–57 DOI: 10.1083/jcb.201112145.

(25) Schmidt, E. K.; Clavarino, G.; Ceppi, M.; Pierre, P. SUnSET, a Nonradioactive Method to Monitor Protein Synthesis. *Nat. Methods* **2009**, *6*, 275–277 DOI: 10.1038/nmeth.1314.

(26) Söderberg, O.; Gullberg, M.; Jarvius, M.; Ridderstråle, K.; Leuchowius, K.-J.; Jarvius, J.; Wester, K.; Hydbring, P.; Bahram, F.; Larsson, L.-G.; Landegren, U. Direct Observation of Individual Endogenous Protein Complexes in Situ by Proximity Ligation. *Nat. Methods* **2006**, *3*, 995–1000 DOI: 10.1038/nmeth947.

(27) tom Dieck, S.; Kochen, L.; Hanus, C.; Heumüller, M.; Bartnik, I.; Nassim-Assir, B.; Merk, K.; Mosler, T.; Garg, S.; Bunse, S.; Tirrell, D. A.; Schuman, E. M. Direct Visualization of Newly Synthesized Target Proteins in Situ. *Nat. Methods* **2015**, *12*, 411–414 DOI: 10.1038/nmeth.3319.

(28) Halstead, J. M.; Lionnet, T.; Wilbertz, J. H.; Wippich, F.; Ephrussi, A.; Singer, R. H.; Chao, J. A. An RNA Biosensor for Imaging the First Round of Translation from Single Cells to Living Animals. *Science* **2015**, *347*, 1367–1370 DOI: 10.1126/science.aaa3380.

(29) Wu, B.; Buxbaum, A. R.; Katz, Z. B.; Yoon, Y. J.; Singer, R. H. Quantifying Protein-mRNA Interactions in Single Live Cells. *Cell* **2015**, *162*, 211–220 DOI: 10.1016/j.cell.2015.05.054.

(30) Katz, Z. B.; English, B. P.; Lionnet, T.; Yoon, Y. J.; Monnier, N.; Ovryn, B.; Bathe, M.; Singer, R. H. Mapping Translation "Hot-Spots" in Live Cells by Tracking Single Molecules of mRNA and Ribosomes. *eLife* **2016**, *5*, e10415 DOI: 10.7554/eLife.10415.

(31) Morisaki, T.; Lyon, K.; Deluca, K. F.; Deluca, J. G.; English, B. P.; Lavis, L. D.; Grimm, J. B.; Viswanathan, S.; Looger, L. L.; Lionnet, T.; Stasevich, T. J. Real-Time Quantification of Single RNA Translation Dynamics in Living Cells. *Science* **2016**, *899*, 1–10 DOI: 10.1126/science.aaf0899.

(32) Wang, C.; Han, B.; Zhou, R.; Zhuang, X. Real-Time Imaging of Translation on Single mRNA Transcripts in Live Cells. *Cell* **2016**, *165*, 990–1001 DOI: 10.1016/j.cell.2016.04.040.

(33) Wu, B.; Eliscovich, C.; Yoon, Y. J.; Singer, R. H. Translation Dynamics of Single mRNAs in Live Cells and Neurons. *Science* **2016**, *1084*, 1–10 DOI: 10.1126/science.aaf1084.

(34) Yan, X.; Hoek, T. A.; Vale, R. D.; Tanenbaum, M. E. Dynamics of Translation of Single mRNA Molecules In Vivo. *Cell* **2016**, *165*, 976–989 DOI: 10.1016/j.cell.2016.04.034.

(35) Pichon, X.; Bastide, A.; Safieddine, A.; Chouaib, R.; Samacoits, A.; Basyuk, E.; Peter, M.; Mueller, F.; Bertrand, E. Visualization of Single Endogenous Polysomes Reveals the Dynamics of Translation in Live Human Cells. *J. Cell Biol.* **2016**, *214*, 769–781 DOI: 10.1083/jcb.201605024.

(36) Rogers, J.; Munro, H. Translation of Ferritin Light and Heavy Subunit mRNAs Is Regulated by Intracellular Chelatable Iron Levels in Rat Hepatoma Cells. *Proc. Natl. Acad. Sci. U. S. A.* **1987**, *84*, 2277–2281 DOI: 10.1073/pnas.84.8.2277.

(37) Rouault, T. A.; Hentze, M. W.; Dancis, A.; Caughman, W.; Harford, J. B.; Klausner, R. D. Influence of Altered Transcription on the Translational Control of Human Ferritin Expression. *Proc. Natl. Acad. Sci. U. S. A.* **1987**, *84*, 6335–6339.

(38) Holmberg, L.; Melander, Y.; Nygård, O. Probing the Structure of Mouse Ehrlich Ascites Cell 5.8S, 18S and 28S Ribosomal RNA in Situ. *Nucleic Acids Res.* **1994**, *22*, 1374–1382 DOI: 10.1093/nar/22.8.1374.

(39) Raj, A.; Bogaard, P. Van Den; Rifkin, S. A.; Oudenaarden, A. Van; Tyagi, S. Imaging Individual mRNA Molecules Using Multiple Singly Labeled Probes. *Nat. Methods* **2008**, *5*, 877–879 DOI: 10.1038/NMETH.1253.

(40) Choi, H. M. T.; Chang, J. Y.; Trinh, L. A.; Padilla, J. E.; Fraser, S. E.; Pierce, N. A. Programmable in Situ Amplification for Multiplexed Imaging of mRNA Expression. *Nat. Biotechnol.* **2010**, *28*, 1208–1212 DOI: 10.1038/nbt.1692.

(41) McConaughy, B. L.; Laird, C. D.; McCarthy, B. J. Nucleic Acid Reassociation in Formamide. *Biochemistry* **1969**, *8*, 3289–3295.

(42) van Holde, K. E. *Chromatin*; Springer Verlag - New York, 1989.

(43) Batish, M.; van den Bogaard, P.; Kramer, F. R.; Tyagi, S. Neuronal mRNAs Travel Singly into Dendrites. *Proc. Natl. Acad. Sci.* **2012**, *109*, 4645–4650 DOI: 10.1073/pnas.1111226109.

(44) Ventoso, I.; Kochetov, A.; Montaner, D.; Dopazo, J.; Santoyo, J. Extensive Translatome Remodeling during ER Stress Response in Mammalian Cells. *PLoS One* **2012**, *7*, 1–12 DOI: 10.1371/journal.pone.0035915.

(45) Blobel, G.; Sabatini, D. Dissociation of Mammalian Polyribosomes into Subunits by Puromycin. *Proc. Natl. Acad. Sci. U. S. A.* **1971**, *68*, 390–394 DOI: 10.1073/pnas.68.2.390.

(46) Cencic, R.; Hall, D. R.; Robert, F.; Du, Y.; Min, J.; Li, L.; Qui, M.; Lewis, L.; Kurtkaya, S.; Dingledine, R.; Fu, H.; Kozakov, D.; Vajda, S.; Pelletier, J. Reversing Chemoresistance by Small Molecule Inhibition of the Translation Initiation Complex eIF4F. *Proc. Natl. Acad. Sci.* **2011**, *108*, 1046–1051 DOI: 10.1073/pnas.1104407108.

(47) Hentze, M. W.; Muckenthaler, M. U.; Andrews, N. C. Balancing Acts: Molecular Control of Mammalian Iron Metabolism. *Cell* **2004**, *117*, 285–297 DOI: 10.1016/S0092-8674(04)00343-5.

(48) Munro, H. N. Iron Regulation of Ferritin Gene Expression. *J. Cell. Biochem.* **1990**, *44*, 107–115 DOI: 10.1002/jcb.240440205.

(49) Torti, F. M.; Torti, S. V. Regulation of Ferritin Genes and Protein. *Blood* **2002**, *99*, 3505–3516 DOI: 10.1182/blood.v99.10.3505.

(50) Zähringer, J.; Baliga, B. S.; Munro, H. N. Novel Mechanism for Translational Control in Regulation of Ferritin Synthesis by Iron. *Proc. Natl. Acad. Sci. U. S. A.* **1976**, *73*, 857–861.

(51) Coccia, E.; Profita, V.; Fiorucci, G. Modulation of Ferritin H-Chain Expression in Friend Erythroleukemia Cells: Transcriptional and Translational Regulation by Hemin. *Mol. Cell. Biol.* **1992**, *12*, 3015–3022 DOI: 10.1128/MCB.12.7.3015.

(52) Iborra, F. J.; Jackson, D. A.; Cook, P. R. The Case for Nuclear Translation. *J. Cell Sci.* **2004**, *117*, 5713–5720 DOI: 10.1242/jcs.01538.

(53) Jung, J.; Lifland, A. W.; Zurla, C.; Alonas, E. J.; Santangelo, P. J. Quantifying RNA-Protein Interactions in Situ Using Modified-MTRIPs and Proximity Ligation. *Nucleic Acids Res.* **2013**, *41*, 1–13 DOI: 10.1093/nar/gks837.

(54) Zhang, W. E. I.; Xie, M.; Shu, M.; Steitz, J. A.; Dimaio, D. A Proximity-Dependent Assay for Specific RNA – Protein Interactions in Intact Cells. *RNA* **2016**, *22*, 1785–1792 DOI: 10.1261/rna.058248.116.7.

(55) Cajigas, J.; Tushev, G.; Will, T. J.; Dieck, S.; Fuerst, N.; Schuman, E. M. The Local Transcriptome in the Synaptic Neuropil Revealed by Deep Sequencing and High-Resolution Imaging. *Neuron* **2012**, *74*, 453–466 DOI: 10.1016/j.neuron.2012.02.036.

(56) Martin, K. C.; Ephrussi, A. mRNA Localization: Gene Expression in the Spatial Dimension. *Cell* **2009**, *136*, 719–730 DOI: 10.1016/j.cell.2009.01.044.

(57) Brandman, O.; Hegde, R. S. Ribosome-Associated Protein Quality Control. *Nat. Struct. Mol. Biol.* **2016**, *23*, 7–15 DOI: 10.1038/nsmb.3147.

(58) Dirks, R. M.; Pierce, N. A. Triggered Amplification by Hybridization Chain Reaction. *Proc. Natl. Acad. Sci. U. S. A.* **2004**, *101*, 15275–15278 DOI: 10.1073/pnas.0407024101.

(59) Mueller, F.; Senecal, A.; Tantale, K.; Marie-nelly, H.; Ly, N.; Collin, O.; Basyuk, E.; Bertrand, E.; Darzacq, X.; Zimmer, C. FISH-Quant : Automatic Counting of Transcripts in 3D FISH Images. *Nat. Methods* **2013**, *10*, 277–278 DOI: 10.1038/nmeth.2406.

(60) Carpenter, A. E.; Jones, T. R.; Lamprecht, M. R.; Clarke, C.; Kang, I. H.; Friman, O.; Guertin, D. A.; Chang, J. H.; Lindquist, R. A.; Moffat, J.; Golland, P.; Sabatini, D. M. CellProfiler: Image Analysis Software for Identifying and Quantifying Cell Phenotypes. *Genome Biol.* **2006**, *7*, R100 DOI: 10.1186/gb-2006-7-10-r100.

(61) Bartschat, A.; Hubner, E.; Reischl, M.; Mikut, R.; Stegmaier, J. XPIWIT - An XML Pipeline Wrapper for the Insight Toolkit. *Bioinformatics* **2016**, *32*, 315–317 DOI: 10.1093/bioinformatics/btv559.

Chapter 3

MONITORING LOCAL MRNA TRANSLATION *IN SITU* IN MOUSE HIPPOCAMPAL NEURONS

3.1 Contributions

The following work was conducted in close collaboration with Sophie Miller and Charlene Kim. Sophie and I performed the FLARIM experiments, and Charlene established the neuron cell cultures. Specifically, Sophie designed the probes for Arc, and I designed those for β-actin and MAP2. Sophie and I jointly performed the RNA/DNA hybridizations and cell preparation for all FLARIM experiments. We also jointly collected images with the confocal microscope. Sophie was responsible for all data analysis of the following work, and I created the final images and figures. Charlene performed all the mice work. She regularly established primary hippocampal neuron cultures from embryonic mice and trained Sophie and me on properly plating the cells onto coverslips and maintaining the cultures before fixation. Charlene also assisted in writing the materials and methods section describing derivation of primary hippocampal cell cultures from embryonic mouse brain.

3.2 Summary

Local translation of mRNA allows cells to establish a localized proteome in a specific subcellular compartment and rapidly modify that proteome in response to external stimuli. The importance of local translation is most apparent in neurons, where dendritic compartments far away from the nucleus must respond quickly to extrinsic signals that are restricted to those compartments. Dendrites and other neuronal processes contain thousands of different mRNAs; however, the regulation of individual mRNAs to produce protein at a particular location, time, or in response to a specific stimulus is not completely understood. We sought to test FLARIM in neuron cultures and apply the technique to characterize transcription and translation of particular mRNAs in these cells. Unlike other methods that have been used to study local translation in neurons, FLARIM is enzyme-free and does not require genetically modified organisms, genetic manipulation of cell cultures, nor application of drugs or modified nucleotides and amino acids. We first demonstrate FLARIM in primary hippocampal neuron cultures by studying β-actin mRNA. We then use FLARIM to characterize the transcriptional and translational upregulation of activity-regulated cytoskeleton-associated protein (Arc) in response to application of Brain-derived neurotrophic factor (BDNF). These experiments illustrate that FLARIM can be applied to other cell types besides fibroblasts in our original work. We also compare the abundance and localization of two MAP2 mRNA isoforms via FISH. In future work, we will apply FLARIM to determine if these isoforms have a differential localization and association with ribosomes in hippocampal neurons under certain environmental conditions.

3.2 Introduction

Neurons are highly compartmentalized cells, with each compartment carrying out specialized functions. The major neuronal cell structures include the soma, axon, and dendrites[1]. The soma is a spherical cytoplasmic region that includes the nucleus and connects to the axon and dendrites. Neurons contain one axon but multiple dendrites, which further branch into multiple processes[2]. The axon is a long, thin extension of uniform width that branches at right angles from the cell body. Dendrites are shorter than the axon and appear thick near the cell body but become gradually thinner as they grow further away from the cell body[3]. The terminal ends of the axon contain synaptic vesicles that release neurotransmitters in response to electrical signals from the soma. The dendrites of neighboring neurons receive these neurotransmitters via receptors on the dendritic spines, which are small membranous protrusions along the length of the dendrite. This interaction forms the synapse: the space between the axon terminal and dendritic spine where signals are transmitted between one neuron to the other[4]. The axon forms the pre-synaptic terminal, and the dendrite forms the post-synaptic terminal[2]. To carry out complex signaling events, which are required for thought processing and autonomic functions, neurons must continually modulate the proteome in their different subcellular compartments.

In vitro metabolic labeling experiments in the 1960s first demonstrated that de novo protein synthesis was possible in neuronal axons and dendrites[5,6]. Subsequently, polyribosomes were discovered at the base of dendritic spines via electron microscopy[7]. Local translation of mRNAs in neurons is now a widely accepted phenomenon, which is mediated by various mechanisms to place specific mRNAs at the proper site for translation[8]. Hundreds to thousands of different mRNAs in a neuron may localize to a specific subcellular site. For example, RNA sequencing has revealed that the axons and dendrites of hippocampal neurons contain over 2,500 different mRNAs[9]. Placing mRNAs in neuronal processes allows neurons to synthesize necessary proteins more quickly in response to

localized signals, as there is no need for these signals to travel to the nucleus to trigger mRNA synthesis and protein export.

Some of the first mRNA transcripts identified to undergo local protein synthesis in neurons include calcium/calmodulin dependent protein kinase II alpha (CamKIIα), activity-regulated cytoskeleton-associated protein (Arc), and β-actin. The local synthesis of each of these transcripts is essential to neuronal function. CamKIIα mRNA localizes to dendrites through cis-acting sequences in its 3' UTR[10,11]. The distal 170 nt of the CamKIIα 3' UTR contain cytoplasmic polyadenylation elements (CPEs) to which the cytoplasmic polyadenylation element binding protein (CPEB) binds. CPEB facilitates dendritic transport as well as polyadenylation and translation of CamKIIα mRNA[12,13]. Local translation of CamKIIα is important for memory formation, as disruption of the 3' UTR sequence in mice results in loss of CamKIIα localization to dendrites and reduced spatial memory, fear conditioning, and object recognition[14]. In comparison to CamKIIα regulation, where transcripts are primed at dendritic outposts for activity-induced translation[15,16], Arc mRNA is rapidly transcribed in response to stimuli and then transported to activated post synaptic sites in dendrites for translation[17,18]. While the mechanism of Arc transcriptional activation is not completely understood, this activation relies on enhancer elements in the Arc promoter[19,20]. For transport into the dendrites, Arc is packaged with several proteins into a messenger ribonucleoprotein (mRNP) particle. The heterogeneous nuclear ribonucleoprotein (hnRNP) A2 binds to a region in the Arc CDS and facilitates kinesin-dependent mRNA transport[21], while fragile-X mental retardation protein (FMRP) and Purα inhibit Arc translation during transport[22,23]. Like CamKIIα, local synthesis of Arc is important for memory formation. Reduction of Arc expression with antisense oligonucleotides impairs long-term potentiation (LTP) and consolidation of spatial memory[24]. Regulation of β-actin mRNA local translation is similar to the regulation of CamKIIα in that a trans-acting protein controls β-actin mRNA movement and expression. Zipcode binding protein 1 (ZBP1) binds β-actin mRNA, translationally represses it, and transports the mRNA to sites for protein synthesis. The

translational repression is relieved and β-actin is finally translated when ZBP1 is phosphorylated by Src kinase[25,26]. This local translation of β-actin is required for neuronal outgrowth and the movement of growth cones in response to attractive extracellular cues[25,27].

Microtubule associated protein 2 (MAP2) mRNA is another one of the initial mRNAs localized to dendrites[28], and MAP2 protein is a well-known marker for dendrites but not axons[29]. However, the local translation of MAP2 mRNA within dendrites has not been completely characterized. MAP2 has two main mRNA isoforms: a low-molecular weight (LMW) isoform and a high-molecular weight (HMW) isoform. The LMW isoform, called MAP2c, is 6 kb long and encodes a protein of 70 kDa. The HMW isoform, called MAP2a/b, is 9 kb long and encodes a protein of 280 kDa[30]. The two isoforms are transcribed from a single gene by alternative splicing. The isoforms differ in their CDS, where MAP2a/b has an additional region that MAP2c lacks. MAP2a/b contains the same CDS sequence as MAP2c but also contains a unique, contiguous sequence of ~3 kb in between the 5' and 3' ends of the MAP2c CDS. The LMW and HMW MAP2 mRNA isoforms appear at different stages of mouse brain development. While MAP2a/b is found in the cerebellum and cerebral hemispheres at all developmental stages, MAP2c is found at significant levels in these regions during only the first 1-2 postnatal weeks[31]. Furthermore, both the mRNA and protein of the MAP isoforms have been shown to occupy different regions of the brain[32]. The differential expression of the MAP2 isoforms suggests that they may have unique functions. It is possible that MAP2 isoform expression differs not only by time and cell type but also by subcellular location. However, the distribution of MAP2 mRNA isoforms within single cells and the local translation of these transcripts have not been characterized.

We sought to visualize and characterize local translation of specific neuronal mRNAs via FLARIM. For this work, we used primary mouse hippocampal neuron cultures. We first validated FLARIM in these neurons by studying β-actin mRNA translation, which we had previously observed by

FLARIM in mouse fibroblasts. As in our original work, we found that significant FLARIM signals appear only when ribosome and mRNA probes are combined but not when either probe is alone. We then used FLARIM to monitor Arc mRNA expression in response to treatment with BDNF, which causes both a transcriptional and translation activation. Finally, we used FISH to compare the expression and localization of different MAP2 mRNA transcripts in cells. The translation of these transcripts will be compared via FLARIM in future work.

3.3 Results and Discussion

As described in Chapter 2, FLARIM utilizes pairs of oligonucleotide probes that bind separately to rRNA and to the mRNA of interest, and that produce strong fluorescence signals via the HCR when in close proximity. We use two types of mRNA probes per transcript of interest: (1) mRNA interaction probes, which target the CDS and pair with the ribosome probes to form binding sites for a linker probe that carries an HCR initiator, and (2) mRNA transcript probes, which target UTRs and separately label the mRNA transcript with a different HCR initiator. The ribosomes probes and mRNA interaction probes contain extension sequences outside of their RNA binding regions. A common extension sequence is used for all mRNA interaction probes, and a different extension sequence is used for all ribosome probes. We use a linker probe that hybridizes to these extension sequences on the mRNA interaction and ribosome probes in order to initiate HCR when the probes are in close proximity. For all of our experiments in neurons, we used the same set of 24 ribosome probes described in Chapter 2. These probes bind to relatively unstructured and chemically accessible regions of the mouse 18S rRNA. Unless otherwise stated, we used the same HCR initiators and fluorescently labeled hairpins as in Chapter 2. We used the B2 HCR initiator and its corresponding hairpins coupled to Alexa Fluor 488 for all mRNA transcript probes, and we used the B3 HCR initiator and its corresponding HCR hairpins coupled to Alexa Fluor 546 to amplify fluorescence signals associated with the linker probe. Signals from the linker probes and from mRNA transcript probes appear as single,

diffraction-limited spots when visualized by confocal microscopy (Fig 3.1B). In the ideal FLARIM scheme, spots that colocalize in the Alexa 488 (shown in red throughout this study) and Alexa 546 (shown in green throughout this study and referred to as 'FLARIM' signals) channels indicate mRNAs bound to ribosomes; spots that appear only in the Alexa 488 channel indicate mRNAs that do not interact with ribosomes. Sequences of all oligonucleotide probes used in this Chapter are listed in Table 3.S1.

We first tested FLARIM in primary mouse hippocampal neurons using probes designed for β-actin mRNA. We used the same set of β-actin mRNA probes described in Chapter 2. Control experiments in which either the mRNA interaction probes or the ribosome probes were omitted showed little or no labeling from the linker probe. However, when both ribosome and mRNA interaction probe sets were added, we saw a significant increase in FLARIM signals from the linker probe (Figure 3.1A) and substantial colocalization of these signals with those derived from the β-actin transcript probes (Figure 3.1C). These results are similar to those obtained in mouse fibroblasts in Chapter 2 and illustrate that the linker washes out of cells when it binds only to an mRNA interaction probe or to a ribosome probe, but it remains stably bound when both probe sets are present. We found on average that 45 ± 6% (n = 8 cells) of β-actin transcripts per cell were colocalized with ribosomes. Colocalized spots appeared in both the cell soma and dendrites (Fig 3.1B). In comparison, the samples with ribosome probes or mRNA interaction probes alone produced punctate Alexa 546 emission to which only 2 ± 1% (n = 9) and 5 ± 2% (n = 8) of Alexa 488 spots colocalized, respectively (Figure 3.1C, Table 3.2). In addition, cells treated with the linker probe alone produced fewer than 10 spots of Alexa 546 emission per cell, and less than 0.5% of Alexa 488 spots colocalized to these Alexa 546 spots (Table 3.2). Hence, the levels of false positive signals arising from nonspecific binding of the linker, or from the HCR amplification step, are negligible.

We next tested the sensitivity of FLARIM to detect changes in mRNA expression in neurons. We chose to study Arc, a well-characterized neuronal

transcript known to undergo both transcriptional and translational regulation in response to neuronal stimulation[18]. In particular, application of BDNF to cultured neurons enhances synthesis of Arc mRNA and protein[33]. In experiments with synaptoneurosomes, which are synaptic vesicles mechanically separated from the cell body, BDNF directly modulates the dendritic translation of Arc[34]. BDNF is a key protein in the family of neurotrophic factors and is involved in neurogenesis, neuron growth and survival, and learning and memory. BDNF modulates gene expression by binding and activating TrkB receptors found on axons, nerve terminals, and dendritic spines. Activated TrkB receptors trigger multiple signaling pathways that lead to the expression of particular mRNAs and proteins[35,36].

We grew neurons to DIV 4-5 and then added BDNF at a final concentration of 100 ng/mL to the cell culture media for 1 h before fixing and processing the cells for FLARIM experiments. We detected a noticeable and statistically significant ($P<0.05$, Student's t-test) increase the in the interaction of Arc mRNA with ribosomes in cells treated with BDNF (Figure 3.2A). After 1 h of treatment, the fraction of Arc mRNAs interacting with ribosomes increased from an average of 3 ± 4% to an average of 16 ± 8% (Figure 3.2B, Table 3.3). The fraction of Arc mRNAs interacting with ribosomes in the untreated samples is comparable to background levels from the control samples where either ribosome or mRNA interaction probes are omitted (Figure 3.2B, Table 3.3). Hence, we conclude that there is no significant translation of Arc in untreated neurons. However, upon stimulation with BNDF, Arc mRNA translation is significantly upregulated.

We also measured the number of Arc mRNAs per cell, which corresponds to the number of mRNA transcript spots detected. In untreated cells, we detected an average of 107 ± 54 Arc mRNAs per cell. In BDNF-treated cells, we detected average of 62 ± 41 Arc mRNAs per cell. This nearly 2-fold increase in the number of Arc mRNAs after BDNF treatment was visibly noticeable but not statistically significant ($P = 0.2411$, Student's t-test). However, this may be due to a limited number of cells analyzed ($n = 4$ cells without BDNF; $n = 6$ cells with BNDF). Additional experiments will be performed to determine if the results are repeatable

and if the observed difference between Arc expression with and without BDNF is statistically significant. Nevertheless, FLARIM reveals distinct increases in Arc mRNA abundance and ribosome association, which are expected after neuronal activation with BDNF. As with our studies of FTH1 in Chapter 2, we demonstrate that FLARIM is useful in assessing both transcriptional and translational control of gene expression in single cells.

We next sought to investigate the local translation of MAP2 mRNA in neurons. MAP2 is a common marker for dendrites but its mRNA translation has not been completely characterized. In particular, MAP2 has two mRNA isoforms, which have unique spatial and temporal expression patterns in the brain[30–32] and may undergo distinct regulation within single cells as well. These mRNA isoforms can be distinguished in single cells via smFISH. The HMW isoform, termed MAP2a/b, contains an additional 3kb region in its CDS compared to the LMW, termed MAP2c. All other sequences between the two isoforms are identical. In order to distinguish these isoforms, we designed three unique mRNA probe sets for MAP2: one set hybridizes to the shared CDS region between the two isoforms (designated “common CDS probes”), a second set hybridizes only to the unique CDS region of the HMW MAP2 isoform (designated “MAP2a/b unique CDS probes”), and a final set hybridizes to the 3’UTR (designated “common 3’UTR probes”), which is identical between the isoforms. Figure 3A illustrates the general locations of these probes along the MAP2 mRNA isoforms. The common CDS probes contain the extension sequence that is used for mRNA interaction probes in FLARIM. These probes can thus to be used to detect ribosome interactions with any MAP2 transcript, regardless of which isoform it is. The MAP2a/b unique CDS probes contain the B1 HCR initiator and were visualized with the corresponding B1 hairpins coupled to Alexa Fluor 647. The common 3’UTR probes contain the B2 HCR initiator and were visualized with the corresponding B2 hairpins coupled to Alexa Fluor 488. To visualize the common CDS probes in smFISH experiments, we used a linker probe that is complementary to 24 nt of the extension sequence, similar to the experiments described in Figure 2.S6 of Chapter 2 and illustrated in

Figure 3.1A. This linker contains the B3 HCR initiator and was visualized with the corresponding B3 hairpins coupled to Alexa 546.

In a smFISH experiment with the above probes, we found that the 71 ± 4% of Alexa 546 spots (from the shared CDS probes) colocalized with Alexa 488 spots (from the common 3'UTR probes). In an ideal smFISH experiment, 100% of fluorescence signals from the shared CDS probes would colocalize with signals from the common 3'UTR probes, as all MAP2 transcripts to contain the sequences targeted by these two probe sets. However, as explained in Chapter 2, fluorescence signals generated by smFISH and smHCR invariably yield less than 100% colocalization for probes targeted to the same message[19,39,43]. In comparison, we found that only 44± 4% of Alexa 546 spots colocalized with Alexa 647 spots (from the MAP2a/b unique CDS probes), suggesting the MAP2 mRNA isoforms are expressed at different levels in hippocampal neurons. Our colocalization results were similar for MAP2 transcripts in the cell soma versus dendrites (Figure 3.6D). In both regions, approximately 70% of Alexa 546 signals from the common CDS probes colocalized to Alexa 488 signals from the 3'UTR probes, and approximately 40% of Alexa 546 signals from the common CDS probes colocalized to Alexa 647 signals from the MAP2a/b unique CDS probes. We will conduct additional experiments to further support these observations. Subsequently, we will conduct FLARIM experiments using the common CDS probes to detect interaction of MAP2 mRNAs with ribosomes. These experiments will illustrate whether the two isoforms display a unique translational regulation in addition to transcriptional regulation.

Various RNA binding proteins mediate the dendritic localization of MAP2 mRNA, but the mechanism by which the two major isoforms are uniquely distributed and expressed is not known. Both MAP2 mRNA isoforms contain a 640-nt dendritic targeting element to which the proteins MARTA1 and MARTA2 bind[37,38]. MARTA2 has been directly implicated in the transport of MAP2 via interaction with the microtubule-based motor KIF5[39]. However, the 3'UTR interactions with MARTA1 and MART2 do not explain how MAP2a/b and MAP2c

localize to different cellular regions, as these transcripts contain an identical 3'UTR. If the MAP2a/b and MAP2c demonstrate a significant difference in their localization patterns, then the additional CDS region of MAP2a/b may provide an additional targeting function. Alternatively, the transcripts may not demonstrate a particular localization pattern but their translation may be modulated based on the presence or absence of the additional CDS region. Another hypothesis is that the transcripts are alternatively spliced after localization. In this case, the additional CDS region may be removed from or retained in MAP2 transcripts based on when and where they will be expressed. Several genes retain introns in their cytoplasmic mRNAs, and while the activity of the spliceosome in the cytoplasm is still debated, these mRNAs may be subject to extranuclear splicing[40]. Splicing factors and components of the spliceosome have been identified in dendrites, and isolated dendrites are capable of splicing reporter pre-mRNAs[41]. A local splicing event of MAP2 would obviate the need to shuttle to the nucleus for processing. Intriguingly, MARTA1 is the homologue of a splicing regulatory protein in humans[42].

3.4 Conclusion and Future Directions

This work shows that our method FLARIM, which visualizes and quantifies changes in ribosome association with endogenous, unmodified mRNAs *in situ* using standard DNA oligonucleotide probes and HCR, can be applied to primary mouse hippocampal neurons. We had previously characterized FLARIM in NIH 3T3 mouse fibroblasts. In working with neurons compared to fibroblasts, we used the same probe design, as well as many of the same sequences, and followed the same FLARIM procedure, excluding slight modifications in the cell fixation and permeabilization steps. This supports that FLARIM can be directly applied to different cell culture systems without significant modifications. In future work, we aim to perform FLARIM experiments in cells from different tissues and species, particularly human, to further support this conclusion. Regardless, FLARIM is designed such that the method is highly tunable. Probe sequences, as well as the

concentration of formamide in buffer and wash solutions, can be easily modified to ensure that HCR amplification occurs essentially only from interacting probe pairs.

In our primary mouse hippocampal neuron cultures, we first demonstrated that FLARIM works in these cells by measuring ribosome-mRNA interactions for β-actin. We then detected increased transcription and ribosome binding to Arc mRNA when cells were treated with BDNF. This demonstrates how FLARIM interrogates both transcription and translation of mRNAs and thus provides unique insights into the nature of gene regulation in single cells. We plan to conduct similar experiments for CamKIIα mRNA, which shows a translational response to BDNF treatment[43]. Finally, we measured the distribution of MAP2 mRNA variants in our neuron cultures. We found that 44% of the MAP2 mRNAs in primary hippocampal neurons are the MAP2a/b isoform, which contains an additional 3 kb region in the CDS region compared to the MAP2c isoform. The remaining MAP2 mRNAs are presumably the MAP2c isoform. Our initial results also suggest that this distribution of MAP2a/b and MAP2c is similar between the soma and dendrites. However, these results reflect a sample of only 11 cells in one experiment. We plan to validate that these results are consistent in repeated experiments. We will then use FLARIM to compare the ribosome association of MAP2 isoforms in hippocampal neurons. FLARIM is well suited to compare the expression of mRNA isoforms that can be distinguished by smFISH. In comparison, methods that require genetic manipulations of mRNA to visualize translation often cannot differentially label unique isoforms produced from the same gene. For instance, current methods that visualize mRNA by tagging its 3'UTR[44–48] would not be able to distinguish the MAP2 variants, which differ in their CDS. The mechanisms that control MAP2 mRNA isoform expression in hippocampal neurons are not completely known, but they may involve RNA binding proteins that uniquely distribute the two variants and or regulate their translation. They may also involve dendritic splicing of localized transcripts, as the known dendritic targeting sequence of MAP2 resides in the 3'UTR that is shared between all variants. Upon characterizing the expression of MAP2 isoforms more

thoroughly in FLARIM experiments, we can use additional molecular biology techniques to understand how the observed expression pattern is accomplished.

In working with neurons, we anticipate that FLARIM will be useful to compare the local translation of mRNAs in different subcellular compartments. Beyond comparing expression of mRNAs in dendrites versus the soma, we may also be able to compare expression in dendritic spines versus the dendritic shaft. The shaft is the long and thin membranous protrusion from the soma, while spines are nodes along the dendritic shaft where dendrites receive information from adjacent neurons[1]. Spines are typically 0.5 – 2 μm in length, 0.01 – 0.8 μm^3 in volume and occupy a density of up to 10 spines per μm along the dendritic shaft in mature neurons[49]. In order to resolve these structures and also enhance the resolution of FLARIM, we can apply expansion FISH (ExFISH)[50] to our samples. With this technique, RNA in cells is covalently attached to a polyelectrolyte gel that is synthesized within the cells. The gel is osmotically swelled, thereby increasing the physical distance between biomolecules and improving the resolution of mRNA imaging by a factor of ~3.3X. ExFISH uses HCR and has been already been applied to mouse brain tissue, supporting that this method will be compatible with FLARIM studies in neurons.

3.5 Acknowledgements

We thank the National Science Foundation Graduate Research Fellowship Program (NSF GRFP, grant number 1144469) and the Programmable Molecular Technology Initiative of the Gordon and Betty Moore Foundation for support of this work. We thank Henry Lester for providing access to his laboratory to collect neurons from mice. We thank Charlene Kim for preparing primary hippocampal neuron cultures and providing feedback on the Methods section of this work. We thank Florian Mueller for development of FISH-quant. We thank Andres Collazo for assistance with the LSM 800 confocal microscope in the Biological Imaging Facility of the Beckman Institute at Caltech.

3.6 Figures

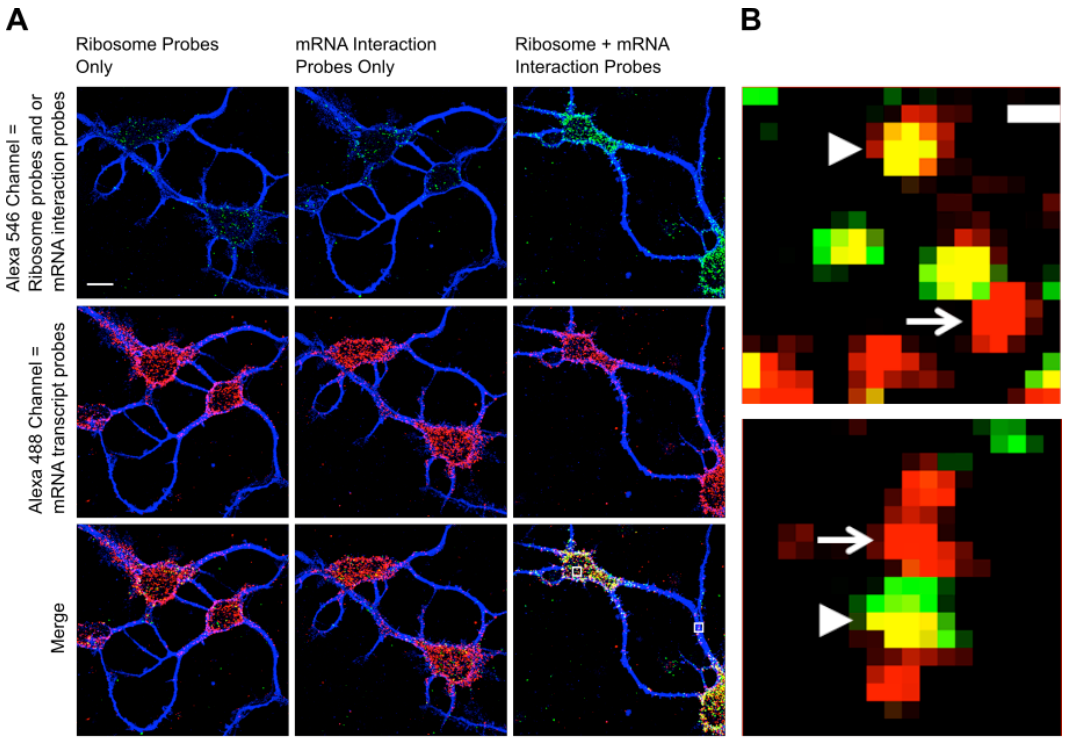
A
Ribosome Probes Only
mRNA Interaction Probes Only
Ribosome + mRNA Interaction Probes
Alexa 546 Channel = Ribosome probes and or mRNA interaction probes
Alexa 488 Channel = mRNA transcript probes
Merge
B

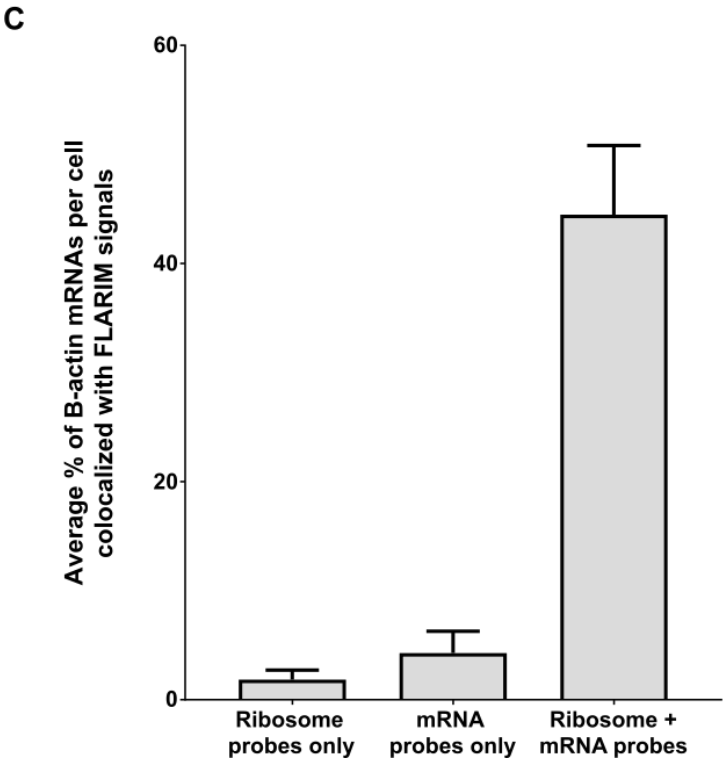
C
Average % of B-actin mRNAs per cell colocalized with FLARIM signals
60
40
20
0
Ribosome probes only
mRNA probes only
Ribosome + mRNA probes

Figure 3.1 (*previous page*): Demonstration of FLARIM in neuron cultures. (A) Primary mouse hippocampal neurons hybridized with either ribosome probes, mRNA interaction probes to β-actin, or both ribosome and β-actin mRNA interaction probes (top, green, Alexa 546 fluorescence). Cells are simultaneously hybridized with β-actin transcript probes (middle, red, Alexa 488 fluorescence). Cell bodies and dendrites are labeled with an anti-MAP2 primary antibody (blue). Merge of ribosome-mRNA interaction signals and transcript signals (bottom). Scale bar = 10 μm. (B) Zoom of single mRNA molecules in the soma (top) and dendrites (bottom). Zoomed-in images correspond to the boxed regions in the merge of the ribosome + mRNA interaction probes picture in (C). Red spot: mRNA transcript without ribosome interaction, indicated by an arrow. Yellow spots: mRNA transcripts with ribosome interaction, indicated by an arrowhead. Scale bar = 0.5 μm. (C) Fraction of β-actin transcript spots colocalized with ribosome-mRNA interaction spots per cell. Error bars, standard deviation.

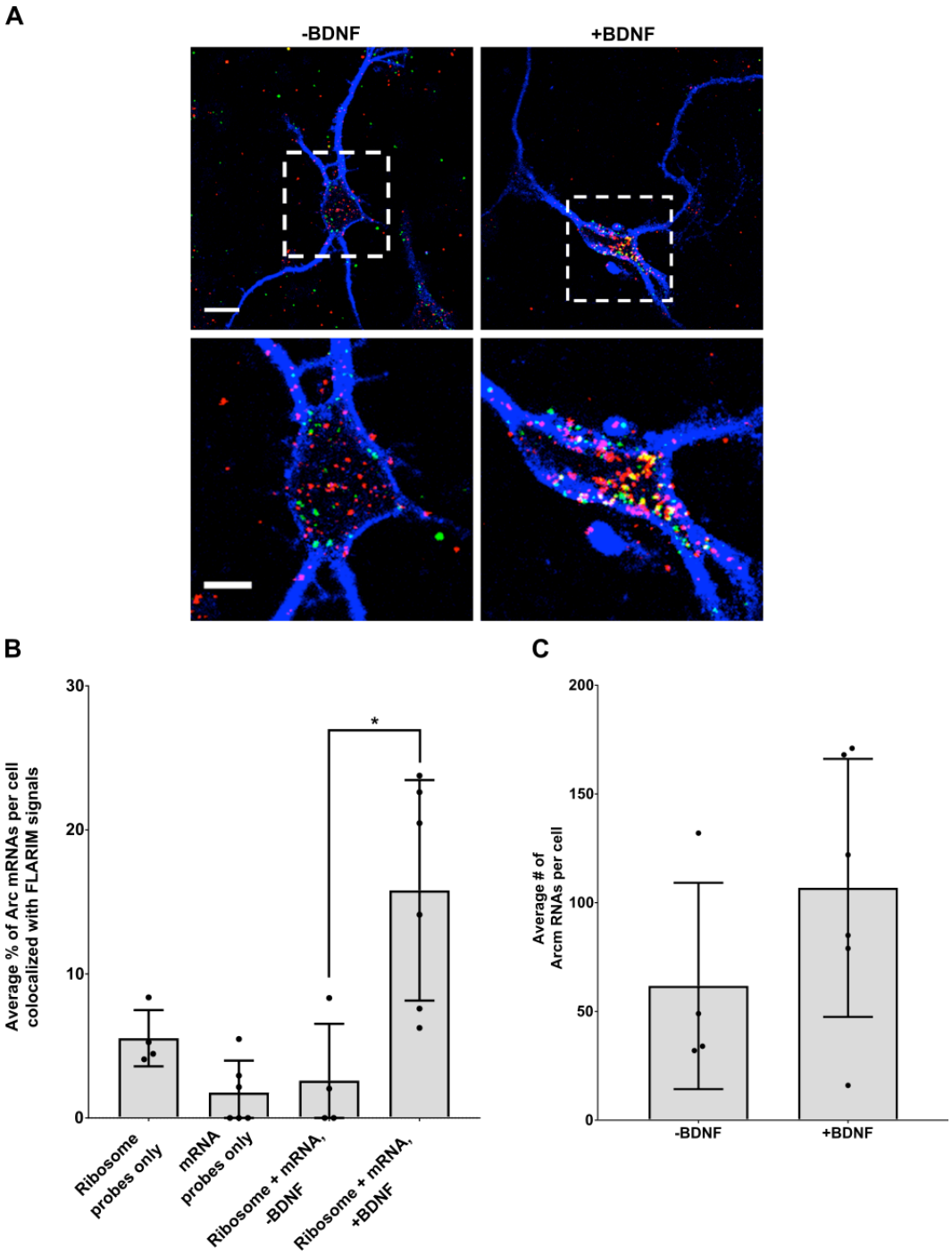
A
-BDNF
+BDNF
B
Average % of Arc mRNAs per cell colocalized with FLARIM signals
30
20
10
0
*
Ribosome probes only
mRNA probes only
Ribosome + mRNA, -BDNF
Ribosome + mRNA, +BDNF
C
Average # of Arcm RNAs per cell
200
150
100
50
0
-BDNF
+BDNF

Figure 3.2 (*previous page*): Changes in Arc mRNA expression in response to added BNDF are detected by FLARIM. (A) Images illustrating increase in ribosome-mRNA interaction for Arc after iron treatment with 100 ng/mL BDNF for 1 h (right) compared to an untreated control (left). In the BDNF-treated sample, there is a noticeable increase in detectable colocalization (yellow) between Arc mRNA transcript signals (red, Alexa 488 fluorescence) and ribosome-mRNA interaction signals (green, Alexa 546 fluorescence). There is also a noticeable increase in the total number of Arc mRNAs (red and yellow spots). Top, scale bar = 10 μm. Bottom, scale bar = 5 μm. (B) Fraction of Arc mRNA transcript spots per cell colocalized with a ribosome-mRNA interaction spot, with and without BDNF treatment. Dots represent single cells. Error bars, standard deviation. *$P < 0.0138$, Student's t-test. (C) Changes in Arc mRNA level per cell, with and without BDNF treatment. Dots represent single cells. Error bars, standard deviation.

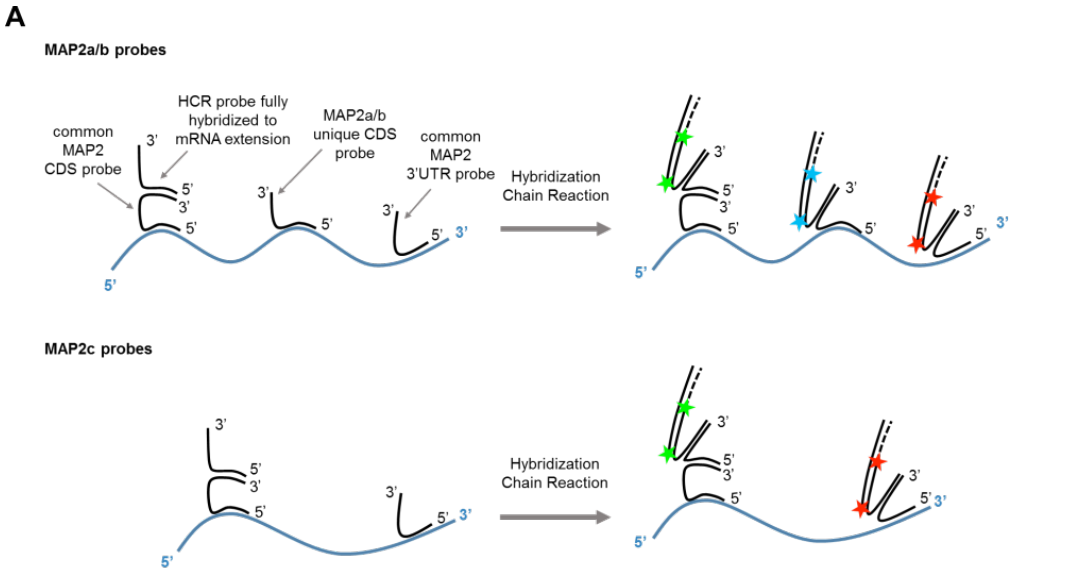
A
MAP2a/b probes
common MAP2 CDS probe
HCR probe fully hybridized to mRNA extension
MAP2a/b unique CDS probe
common MAP2 3'UTR probe
Hybridization Chain Reaction
MAP2c probes
Hybridization Chain Reaction

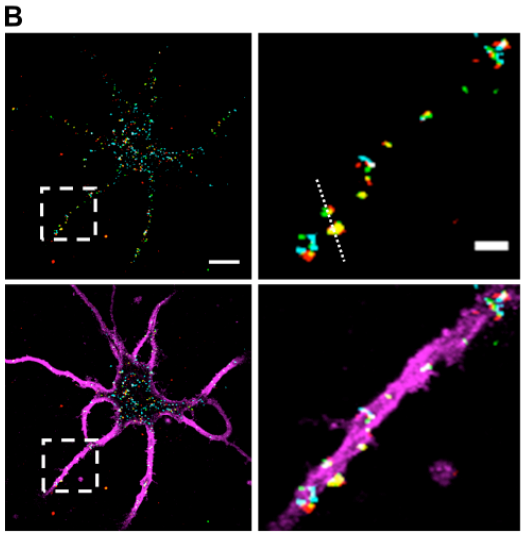
B

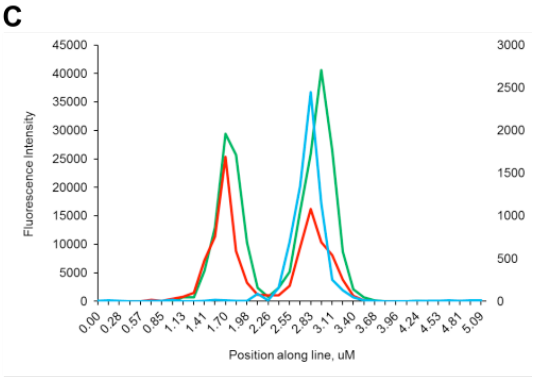
C
Fluorescence Intensity
Position along line, uM

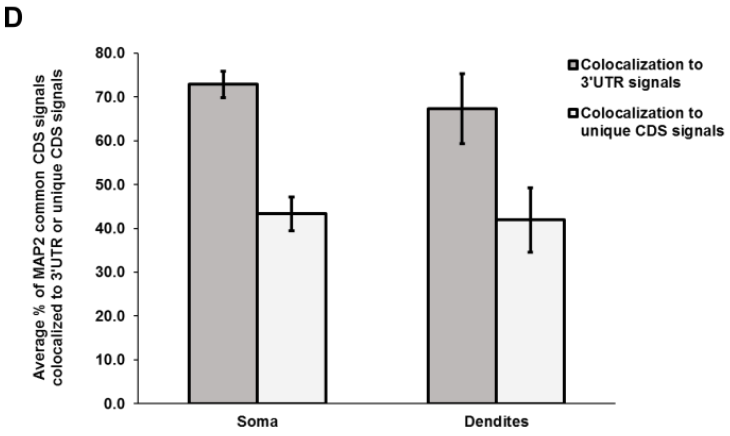
D
Average % of MAP2 common CDS signals colocalized to 3'UTR or unique CDS signals
Colocalization to 3'UTR signals
Colocalization to unique CDS signals
Soma
Dendites

Figure 3.3 (*previous page*): smFISH detection of MAP2 mRNA isoforms in neurons. (A) Schematic of the smFISH probe design for MAP2a/b (top) and Map2c (bottom). MAP2a/b contains an additional 3 kb sequences in its CDS compared to MAP2c. This region can be targeted with a unique set of probes and fluorophore. Hence, MAP2a/b mRNAs are identified by the colocalization of three fluorescent spots: green (Alexa 546), cyan (Alexa 647), and red (Alexa 488). MAP2c is identified by the colocalization of two fluorescent spots: green (Alexa 546) and red (Alexa 488). (B) Confocal image of MAP2 smFISH in a primary hippocampal neuron culture. Boxed regions in the images on the left are zoomed in to create the images on the right. Bottom images are a merge with MAP2 antibody staining (magenta). Left, scale bar = 10 μm. Right, scale bar = 2 μm. (C) Fluorescence profile of the line drawn through spots in the top right image of (B). The profile shows fluorescence intensities of each fluorophore from left to right along the line. The spot on the left demonstrates colocalization between green and red, indicating MAP2c. The spot on the right demonstrates colocalization between green, cyan, and red, indicating MAP2a/b. The left vertical axis reflects fluorescence intensities of Alexa 488 and Alexa 546. The right vertical axis reflects the fluorescence intensity of Alexa 647.

3.7 Tables

Table 3.1: Sequences of all oligonucleotide probes used in Chapter 3. Provided as a separate Excel file.

Table 3. 2: Fraction (average ± standard deviation) of putative β-actin transcripts (Alexa 488 spots) in mouse hippocampal neuron preparations colocalized with Alexa 546 spots, which may correspond to linker probes or dye-labeled HCR hairpins, when only β-actin interaction probes, only ribosomes probes, or neither are added. n = 3-6 cells per measurement.

Ribosome probes only	β-actin mRNA interaction probes only	Neither ribosome nor mRNA interaction probes (Linker + HCR background)
0.02 ± 0.01	0.05 ± 0.02	0.002 ± 0.002

Table 3. 3: Fraction (average ± standard deviation) of putative Arc transcripts (Alexa 488 spots) in mouse hippocampal neuron preparations colocalized with Alexa 546 spots, which may correspond to linker probes or dye-labeled HCR hairpins, when Arc interaction probes, ribosomes probes, or both are omitted. n = 3-6 cells per measurement.

Ribosome probes only	Arc mRNA interaction probes only	Neither ribosome nor mRNA interaction probes (Linker + HCR background)
0.06 ± 0.02	0.02 ± 0.02	0.003 ± 0.003

Table 3.4: Fraction of ribosome-mRNA interaction spots colocalized with Arc mRNA transcript spots with or without BDNF treatment. Data represent two independent experiments. n = 4-6 cells per measurement per experiment.

	Fraction of spots
Control	0.03 ± 0.04
BDNF	0.16 ± 0.08

3.8 Methods

Neurobasal medium (Gibco, #21103-049), GlutaMAX (Gibco, #35050-061), B27 (Gibco, #17504-044), Donor Equine Serum (SH30074.03) and HBSS (Gibco, #14175-095) were purchased from Thermo Fisher Scientific (Carlsbad, CA). SecureSeal hybridization chambers (8 well, 7mm x 7mm x 0.8mm, SKU 621503) were purchased from Grace BioLabs (Bend, OR). Multiwell cell culture plates (6-well, #10062-892) and 22mm x 22mm No. 2 glass coverslips (#48368-062) were purchased from VWR (Brisbane, CA). All DNA oligonucleotide probes were designed using Stellaris Probe Designer version 4.2 (LGC Biosearch Technologies) and purchased from Integrated DNA Technologies (San Diego, CA). HCR hairpins were purchased pre-coupled to fluorophores from Molecular Instruments (Pasadena, CA). Formamide (SKU F9037), dextran sulfate (SKU D8906), Triton X-100 (SKU T8797), poly-D-lysine hydrobromide (SKU P6407), poly-L-ornithine (SKU P4957), laminin (SKU L2020), brain-derived human neurotrophic factor (BDNF) (SKU B3795), L-Ascorbic acid (SKU A7506), DNAse I (SKU DN25), and BSA (SKU A7030) were purchased from Sigma-Aldrich (St. Louis, MO). Papain was purchased from Worthington Biochemical Corporation (Lakewood, NJ). 16% paraformaldehyde (#15710) was purchased from Electron Microscopy Sciences. A primary antibody for MAP2 (ab32454) and a donkey anti-rabbit IgG secondary antibody coupled to Alexa 405 (ab175651) were purchased from Abcam (Burlingame, CA).

Images were acquired on a Zeiss LSM 800 laser scanning confocal microscope operated by the Biological Imaging Facility of the Beckman Institute at Caltech. Imaging data were analyzed with the FISH-quant program written by Florian Mueller.

Derivation of Primary Hippocampal Cell Cultures from Embryonic Mouse Brain. Prior to obtaining cells, coverslips were rinsed with 70% EtOH, dried, placed into single wells of 6-well plates, and finally sterilized under UV light for 10-15 min. The coverslips were then coated with 0.1 mg/mL poly-D-lysine

overnight at 37˚C. The following morning, poly-D-lysine was aspirated from the coverslips, which were then coated with poly-L-ornithine for 1 h at 37˚C, rinsed twice with sterile water, and coated with 0.01 mg/mL laminin for at least 1 h at 37˚C before plating cells.

A pregnant mouse was euthanized on gestational day 16 using CO_2. The abdomen of the euthanized mouse was sprayed with 70% EtOH and cut laterally and proximally on both sides. The uterus was removed from the abdomen by cutting the ends of the uterine horn and was placed in a petri dish in a sterile hood. The embryo sac was removed from the uterus, and the embryonic mice were decapitated by pinching at the neck with forceps. For each mouse, the skin and skull surrounding the brain were removed with forceps, and the forebrain was removed and placed in a petri dish with cold HBSS under a dissecting microscope. Meninges and vasculature were removed, and the hippocampus was isolated and cut with forceps into four sections of roughly equal size.

The quartered hippocampal sections were placed into a 15 mL conical tube. After the sections settled, HBSS was removed and 500 µL of 15 units/mL papain in HBSS was added to the tube. The tube was placed into a water bath at 37˚C for 15 min. Cells then resuspended by flicking the tube after 7.5 min. The hippocampal sections were then pipetted into a 1 mL solution of 1 mg/mL DNase and allowed to settle to the bottom of the tube. The sections were then rinsed by transferring them into a 15 mL tube containing 1 mL of 10% donor equine in HBSS. This rinse was repeated after allowing the sections to settle to the bottom of the tube. The cells were then triturated by pipetting up and down 7 times. A 200-µL aliquot of 4& BSA was slowly pipetted into the bottom of the tube. The cells were then centrifuged at 280 x g for 6 min. The supernatant was aspirated, and the cells were resuspended in 1 mL of Neurobasal medium supplemented with 0.5 mM GlutaMAX and 1% donor equine serum (plating medium). Cells were counted with a hemocytometer, and the cell suspension was diluted to 600 cells/µL with plating medium.

For plating cells, laminin was aspirated from the coated coverslips in batches of two coverslips at a time. Cells were plated onto the coverslips immediately after aspirating in order to prevent coverslips from drying out. 1 mL of cells at a density of 6 x 10^5 cells/coverslip was added to each well. After 1 h, 2 mL of plating medium supplemented with B27 (diluted by 50X) and 17.6 mg/mL ascorbic acid (culture medium) was added to each well. The final primary hippocampal neuron cultures were grown at 37˚C in 5% CO_2. Half of the medium in each well was exchanged with fresh culture medium every 2-4 days.

***In Situ* Hybridization and Hybridization Chain Reaction (HCR)**. Primary hippocampal neurons were fixed at DIV 4-5 with 4% formaldehyde, 5% sucrose in 1X PBS for 20 min at room temperature (25°C). For neuronal stimulation experiments, cells were incubated with BDNF at 100 ng/mL for 1 h at 37˚C and 5% CO_2 prior to fixing. After fixation, cells were washed three times with 1X PBS. Fixed cells were permeabilized with 0.1% Triton in 1X PBS for 10 min with gentle rocking. Cells were then washed three times with 1X PBS. Cells were stored in 70% ethanol at 4˚C for at least 2 h and up to 2 days before hybridization.

For hybridization, coverslips were removed from ethanol and air dried. Secure-Seal hybridization chambers were attached to each coverslip. Cells were incubated overnight at 37˚C in a humid chamber with 1-2 nM/oligo of probes for ribosomes and mRNA in a hybridization buffer of 10% formamide and 10% dextran sulfate in 2X SSC.

The next day, the probe solutions were removed, and cells were washed three times with a solution of 35% formamide and 0.1% Triton in 2X SSC, then three times with 2X SSC, to remove excess probes not bound to RNA. Cells were then incubated for 30 min at 40˚C with a pre-heated solution of 10 nM linker probe in a hybridization buffer consisting of 35% formamide and 10% dextran sulfate in 2X SSC (“linker hybridization buffer”). After incubation, cells were washed three times with 0.1% Triton in 2X SSC and twice with 2X SSC, then were left to cool

for 15-20 min at room temperature. Cells were finally washed three times with 35% formamide and 0.1% Triton in 2X SSC and three times with 2X SSC to remove any unbound or partially-hybridized linker probes.

For HCR, the basic protocol of Choi and coworkers was followed with modifications[51]. Fluorescently labeled HCR hairpins were first snap-cooled (heated to 95˚C for 90 sec, then allowed to cool at room temperature for 30 min). The cells were then incubated for 1 h at room temperature (25˚C) with 85 nM hairpins in a hybridization buffer of 10% dextran sulfate in 2X SSC. Following HCR, the cells were washed twice with 0.1% Triton in 2X SSC, incubated with 1 μg/mL DAPI for 1 min, washed twice with 2X SSC, and then kept in 2X SSC for imaging.

Antibody Staining. After RNA *in situ* hybridization and HCR, cells were stained with a MAP2 antibody to label dendrites. Cells were first blocked with 1% BSA in PBS at room temperature for 30 min. The cells were then incubated with a primary polyclonal anti-MAP2 antibody at a final concentration of 10 μg/mL in 1% BSA for 1 h. The primary antibody solution was removed, and the cells were washed three times with 1X PBS. The cells were then incubated with a secondary IgG antibody coupled to Alexa 405 at a final concentration of 4 μg/mL in 1% BSA for 1 h. The secondary antibody solution was removed, and the cells were washed three times with 1X PBS. Cells were kept in PBS for imaging.

Fluorescence Imaging. All images were collected with a Zeiss LSM 800 laser scanning confocal microscope, using a 63X, NA 1.4 Plan-Apochromat objective. Resolution was set to 1024 x 1024 with a digital zoom of 0.7X and line averaging of 2. Excitation laser sources and emission ranges were 405 nm/400-510 nm (Alexa 405, shown as blue or magenta), 488 nm/510-560 nm (Alexa 488, shown as red), 561 nm/560-700 nm (Alexa 546, shown as green), and 650 nm (Alexa 647, shown as cyan). Each image was collected as a 3D stack of 15-30 images with a spacing of 0.4 μm in the z-direction between slices.

Image Analysis. Images were analyzed using the MATLAB-based program FISH-

quant[52]. Outlines of cells and nuclei were drawn manually in FISH-quant. A 3D dual-Gaussian filter was used in FISH-quant for background subtraction. Spots corresponding to ribosome-mRNA interactions or mRNA transcripts were identified by fitting with a 3D Gaussian function. The intensity and the width of the 3D Gaussian were thresholded to exclude autofluorescence and non-specific signals. Ribosome-mRNA interaction spots and mRNA transcript spots were identified independently and then analyzed for colocalization. The distance threshold for colocalization was set at 420 nm, which is equal to 3 pixels in all of our images. Raw intensity values were used for measurements of fluorescence intensity.

3.9 References

(1) Rangaraju, V.; Dieck, S.; Schuman, E. M. Local Translation in Neuronal Compartments : How Local Is Local? *EMBO Rep.* **2017**, 1–19.

(2) Craig, A. M.; Banker, G. Neuronal Polarity. *Annu. Rev. Neurosci.* **1994**, *17* (1), 267–310 DOI: 10.1146/annurev.ne.17.030194.001411.

(3) Fukata, Y.; Kimura, T.; Kaibuchi, K. Axon Specification in Hippocampal Neurons. *Neurosci. Res.* **2002**, *43*, 305–315 DOI: 10.1016/S0168-0102(02)00062-7.

(4) Arimura, N.; Kaibuchi, K. Neuronal Polarity: From Extracellular Signals to Intracellular Mechanisms. *Nat. Rev. Neurosci.* **2007**, *8* (3), 194–205 DOI: 10.1038/nrn2056.

(5) Koenig, E. Synthetic Mechanisms in the Axon-IV. in Vitro Incorporation of [3H]Precursors Into Axonal Protein and RNA. *J. Neurochem.* **1967**, *14*, 437–446 DOI: 10.1111/j.1471-4159.1967.tb09542.x.

(6) Giuditta, A.; Dettbar, W. D.; Brzin, M. Protein Synthesis in the Isolated Giant Axon of the Squid. *Biochemistry* **1968**, *59*, 1284–1287.

(7) Steward, O.; Levy, W. B. Preferential Localization of Polyribosomes under the Base of Dendritic Spines in Granule Cells of the Dentate Gyrus. *J Neurosci* **1982**, *2*, 284–291 DOI: 0270-6474/82/0203-0284.

(8) Martin, K. C.; Ephrussi, A. mRNA Localization: Gene Expression in the Spatial Dimension. *Cell* **2009**, *136*, 719–730 DOI: 10.1016/j.cell.2009.01.044.

(9) Cajigas, J.; Tushev, G.; Will, T. J.; Dieck, S.; Fuerst, N.; Schuman, E. M. The Local Transcriptome in the Synaptic Neuropil Revealed by Deep Sequencing and High-Resolution Imaging. *Neuron* **2012**, *74*, 453–466 DOI: 10.1016/j.neuron.2012.02.036.

(10) Mayford, M.; Baranes, D.; Podsypanina, K.; Kandel, E. R. The 3'-untranslated Region of CaMKII Is a Cis-Acting Signal for the Localization and Translation of mRNA in Dendrites. *Proc. Natl. Acad. Sci.* **1996**, *93*, 13250–13255 DOI: 10.1073/pnas.93.23.13250.

(11) Mori, Y.; Imaizumi, K.; Katayama, T.; Yoneda, T.; Tohyama, M. Two Cis-Acting Elements in the 3' Untranslated Region of Alpha-CaMKII Regulate Its Dendritic Targeting. *Nat. Neurosci.* **2000**, *3*, 1079–1084 DOI: 10.1038/80591.

(12) Wu, L.; Wells, D.; Tay, J.; Mendis, D.; Abbott, M. A.; Barnitt, A.; Quinlan, E.; Heynen, A.; Fallon, J. R.; Richter, J. D. CPEB-Mediated Cytoplasmic Polyadenylation and the Regulation of Experience-Dependent Translation of a-CaMKII mRNA at Synapses. *Neuron* **1998**, *21*, 1129–1139 DOI: 10.1016/S0896-6273(00)80630-3.

(13) Huang, Y. S.; Carson, J. H.; Barbarese, E.; Richter, J. D. Facilitation of Dendritic mRNA Transport by CPEB. *Genes Dev.* **2003**, *17* (5), 638–653 DOI: 10.1101/gad.1053003.

(14) Miller, S.; Yasuda, M.; Coats, J. K.; Jones, Y.; Martone, M. E.; Mayford, M. Disruption of Dendritic Translation of CaMKIIalpha Impairs Stabilization of Synaptic Plasticity and Memory Consolidation. *Neuron* **2002**, *36*, 507–519 DOI: 10.1016/S0896-6273(02)00978-9.

(15) Ouyang, Y.; Rosenstein, A.; Kreiman, G.; Schuman, E. M.; Kennedy, M. B. Tetanic Stimulation Leads to Increased Accumulation of Ca2+/Calmodulin-Dependent Protein Kinase II via Dendritic Protein Synthesis in Hippocampal Neurons. *J. Neurosci.* **1999**, *19*, 7823–7833.

(16) Bagni, C.; Mannucci, L.; Dotti, C. G.; Amaldi, F. Chemical Stimulation of Synaptosomes Modulates Alpha -Ca2+/calmodulin-Dependent Protein Kinase II mRNA Association to Polysomes. *J Neurosci* **2000**, *20*, 1–6 DOI: 20004207 [pii].

(17) Steward, O.; Wallace, C. S.; Lyford, G. L.; Worley, P. F. Synaptic Activation Causes the mRNA for the IEG Arc to Localize Selectively near Activated Postsynaptic Sites on Dendrites. *Neuron* **1998**, *21*, 741–751.

(18) Bramham, C. R.; Alme, M. N.; Bittins, M.; Kuipers, S. D.; Nair, R. R.; Pai, B.; Panja, D.; Schubert, M.; Soule, J.; Tiron, A.; Wibrand, K. The Arc of Synaptic Memory. *Exp. Brain Res.* **2010**, *200*, 125–140 DOI:

10.1007/s00221-009-1959-2.

(19) Pintchovski, S. A.; Peebles, C. L.; Joo Kim, H.; Verdin, E.; Finkbeiner, S. The Serum Response Factor and a Putative Novel Transcription Factor Regulate Expression of the Immediate-Early Gene Arc/Arg3.1 in Neurons. *J. Neurosci.* **2009**, *29*, 1525–1537 DOI: 10.1523/JNEUROSCI.5575-08.2009.

(20) Kawashima, T.; Okuno, H.; Nonaka, M.; Adachi-morishima, A.; Kyo, N.; Okamura, M.; Takemoto-Kimura, S.; Worley, P. F.; Bito, H. Synaptic Activity-Responsive Element in the Arc / Arg3 . 1 Promoter Essential for Synapse-to-Nucleus Signaling in Activated Neurons. *PNAS* **2009**, *106*, 316–321.

(21) Gao, Y.; Tatavarty, V.; Korza, G.; Levin, M.; Carson, J. Multiplexed Dendritic Targeting of α Calcium Calmodulin-Dependent Protein Kinase II, Neurogranin, and Activity-Regulated Cytoskeleton-Associated Protein RNAs by the A2. *Mol. Biol. Cell* **2008**, *19*, 2311–2327 DOI: 10.1091/mbc.E07–09–0914.

(22) Zalfa, F.; Zalfa, F.; Giorgi, M.; Giorgi, M.; Primerano, B.; Primerano, B.; Moro, A.; Moro, A.; Penta, A. Di; Penta, A. Di; Reis, S.; Reis, S.; Oostra, B.; Oostra, B.; Bagni, C.; Bagni, C.; Lucia, F. S.; Lucia, F. S.; Ardeatina, V.; Ardeatina, V. The Fragile X Syndrome Protein FMRP Associates with. *Cell* **2003**, *112*, 317–327.

(23) Kanai, Y.; Dohmae, N.; Hirokawa, N. Kinesin Transports RNA: Isolation and Characterization of an RNA-Transporting Granule. *Neuron* **2004**, *43* (4), 513–525 DOI: 10.1016/j.neuron.2004.07.022.

(24) Guzowski, J. F.; Lyford, G. L.; Stevenson, G. D.; Houston, F. P.; McGaugh, J. L.; Worley, P. F.; Barnes, C. A. Inhibition of Activity-Dependent Arc Protein Expression in the Rat Hippocampus Impairs the Maintenance of Long-Term Potentiation and the Consolidation of Long-Term Memory. *J. Neurosci.* **2000**, *20*, 3993–4001 DOI: 20/11/3993 [pii].

(25) Hüttelmaier, S.; Zenklusen, D.; Lederer, M.; Dictenberg, J.; Lorenz, M.; Meng, X.; Bassell, G. J.; Condeelis, J.; Singer, R. H. Spatial Regulation of β-

Actin Translation by Src-Dependent Phosphorylation of ZBP1. *Nature* **2005**, *438*, 512–515 DOI: 10.1038/nature04115.

(26) Welshhans, K.; Bassell, G. J. Netrin-1-Induced Local Beta-Actin Synthesis and Growth Cone Guidance Requires Zipcode Binding Protein 1. *J. Neurosci.* **2011**, *31*, 9800–9813 DOI: 10.1523/JNEUROSCI.0166-11.2011.

(27) Yao, J.; Sasaki, Y.; Wen, Z.; Bassell, G. J.; Zheng, J. Q. An Essential Role for β-Actin mRNA Localization and Translation in Ca2+-Dependent Growth Cone Guidance. *Nat. Neurosci.* **2006**, *9*, 1265–1273 DOI: 10.1038/nn1773.

(28) Garner, C. C.; Tucker, R. P.; Matus, A. Selective Localization of Messenger RNA for Cytoskeletal MAP2 in Dendrites. *Nature* **1988**, *336*, 674–677 DOI: 10.1038/332141a0.

(29) Kosik, K. S.; Finch, E. A. MAP2 and Tau Segregate into Dendritic and Axonal Domains after the Elaboration of Morphologically Distinct Neurites: An Immunocytochemical Study of Cultured Rat Cerebrum. *J. Neurosci.* **1987**, *7*, 3142–3153.

(30) Papandrikopoulou, A.; Doll, T.; Tucker, R.; Garner, C.; Matus, A. Embryonic MAP2 Lacks the Crosslinking Sidearm Sequences and Dendritic Targeting Signal of Adult MAP2. *Nature* **1989**, *340*, 650–652 DOI: 10.1038/340301a0.

(31) Charrierebertrand, C.; Garner, C.; Tardy, M.; Nunez, J. Expression of Various Microtubule-Associated Protein-2 Forms in the Developing Mouse-Brain and in Cultured Neurons and Astrocytes. *J. Neurochem.* **1991**, *56*, 385–391.

(32) Fujimori, K.; Takauji, R.; Tamamaki, N. Differential Localization of High- and Low-Molecular-Weight Variants of Microtubule-Associated Protein 2 in the Developing Rat Telencephalon. *J. Comp. Neurol.* **2002**, *449* (4), 330–342 DOI: 10.1002/cne.10286.

(33) Messaoudi, E.; Kanhema, T.; Soule, J.; Tiron, A.; Dagyte, G.; da Silva, B.; Bramham, C. R. Sustained Arc/Arg3.1 Synthesis Controls Long-Term Potentiation Consolidation through Regulation of Local Actin

Polymerization in the Dentate Gyrus In Vivo. *J. Neurosci.* **2007**, *27*, 10445–10455 DOI: 10.1523/JNEUROSCI.2883-07.2007.

(34) Yin, Y.; Edelman, G. M.; Vanderklish, P. W. The Brain-Derived Neurotrophic Factor Enhances Synthesis of Arc in Synaptoneurosomes. *Proc. Natl. Acad. Sci.* **2002**, *99*, 2368–2373 DOI: 10.1073/pnas.042693699.

(35) Binder, D. K.; Scharfman, H. E. Mini Review: Brain-Derived Neurotrophic Factor. *Growth Factors* **2004**, *22*, 123–131 DOI: 10.1080/08977190410001723308.

(36) Leal, G.; Comprido, D.; Duarte, C. B. BDNF-Induced Local Protein Synthesis and Synaptic Plasticity. *Neuropharmacology* **2014**, *76* (PART C), 639–656 DOI: 10.1016/j.neuropharm.2013.04.005.

(37) Blichenberg, a; Schwanke, B.; Rehbein, M.; Garner, C. C.; Richter, D.; Kindler, S. Identification of a Cis-Acting Dendritic Targeting Element in MAP2 mRNAs. *J. Neurosci.* **1999**, *19* (20), 8818–8829.

(38) Rehbein, M.; Kindler, S.; Horke, S.; Richter, D. Two Trans-Acting Rat-Brain Proteins, MARTA1 and MARTA2, Interact Specifically with the Dendritic Targeting Element in MAP2 mRNAs. *Mol. Brain Res.* **2000**, *79* (1–2), 192–201 DOI: 10.1016/S0169-328X(00)00114-5.

(39) Zivraj, K. H.; Rehbein, M.; Ölschläger-Schütt, J.; Schob, C.; Falley, K.; Buck, F.; Schweizer, M.; Schepis, A.; Kremmer, E.; Richter, D.; Kreienkamp, H. J.; Kindler, S. The RNA-Binding Protein MARTA2 Regulates Dendritic Targeting of MAP2 mRNAs in Rat Neurons. *J. Neurochem.* **2013**, *124*, 670–684 DOI: 10.1111/jnc.12079.

(40) Buckley, P. T.; Khaladkar, M.; Kim, J.; Eberwine, J. Cytoplasmic Intron Retention, Function, Splicing, and the Sentinel RNA Hypothesis. *Wiley Interdiscip. Rev. RNA* **2014**, *5*, 223–230 DOI: 10.1002/wrna.1203.

(41) Glanzert, J.; Miyashirot, K. Y.; Sulo, J.; Barrett, L.; Beltt, B.; Haydon, P.; Eberwinett, J. RNA Splicing Capability of Live Neuronal Dendrites. *PNAS* **2005**, *102* (46), 16859–16864.

(42) Rehbein, M.; Wege, K.; Buck, F.; Schweizer, M.; Richter, D.; Kindler, S.

Molecular Characterization of MARTA1, a Protein Interacting with the Dendritic Targeting Element of MAP2 mRNAs. *J. Neurochem.* **2002**, *82* (5), 1039–1046 DOI: 10.1046/j.1471-4159.2002.01058.x.

(43) Aakalu, G.; Smith, W. B.; Nguyen, N.; Jiang, C.; Schuman, E. M. Dynamic Visualization of Local Protein Synthesis in Hippocampal Neurons. *Neuron* **2001**, *30*, 489–502 DOI: 10.1016/S0896-6273(01)00295-1.

(44) Morisaki, T.; Lyon, K.; Deluca, K. F.; Deluca, J. G.; English, B. P.; Lavis, L. D.; Grimm, J. B.; Viswanathan, S.; Looger, L. L.; Lionnet, T.; Stasevich, T. J. Real-Time Quantification of Single RNA Translation Dynamics in Living Cells. *Science* **2016**, *899*, 1–10 DOI: 10.1126/science.aaf0899.

(45) Wang, C.; Han, B.; Zhou, R.; Zhuang, X. Real-Time Imaging of Translation on Single mRNA Transcripts in Live Cells. *Cell* **2016**, *165*, 990–1001 DOI: 10.1016/j.cell.2016.04.040.

(46) Wu, B.; Eliscovich, C.; Yoon, Y. J.; Singer, R. H. Translation Dynamics of Single mRNAs in Live Cells and Neurons. *Science* **2016**, *1084*, 1–10 DOI: 10.1126/science.aaf1084.

(47) Yan, X.; Hoek, T. A.; Vale, R. D.; Tanenbaum, M. E. Dynamics of Translation of Single mRNA Molecules In Vivo. *Cell* **2016**, *165*, 976–989 DOI: 10.1016/j.cell.2016.04.034.

(48) Pichon, X.; Bastide, A.; Safieddine, A.; Chouaib, R.; Samacoits, A.; Basyuk, E.; Peter, M.; Mueller, F.; Bertrand, E. Visualization of Single Endogenous Polysomes Reveals the Dynamics of Translation in Live Human Cells. *J. Cell Biol.* **2016**, *214*, 769–781 DOI: 10.1083/jcb.201605024.

(49) Hering, H.; Sheng, M. Dendritic Spines: Structure, Dynamics and Regulation. *Nat. Rev. Neurosci.* **2001**, *2*, 880–888.

(50) Chen, F.; Wassie, A. T.; Cote, A. J.; Sinha, A.; Alon, S.; Asano, S.; Daugharthy, E. R.; Chang, J.-B.; Marblestone, A.; Church, G. M.; Raj, A.; Boyden, E. S. Nanoscale Imaging of RNA with Expansion Microscopy. *Nat. Methods* **2016**, *13*, 679–684 DOI: 10.1038/nmeth.3899.

(51) Choi, H. M. T.; Beck, V. A.; Pierce, N. A. Next-Generation in Situ

Hybridization Chain Reaction : Higher Gain , Lower Cost , Greater Durability. *ACS Nano* **2014**, *8*, 4284–4294 DOI: 10.1021/nn405717p C2014.

(52) Mueller, F.; Senecal, A.; Tantale, K.; Marie-nelly, H.; Ly, N.; Collin, O.; Basyuk, E.; Bertrand, E.; Darzacq, X.; Zimmer, C. FISH-Quant : Automatic Counting of Transcripts in 3D FISH Images. *Nat. Methods* **2013**, *10*, 277–278 DOI: 10.1038/nmeth.2406.